Caveats on tomographic images

Gillian R. Foulger[1], Giuliano F. Panza[2], Irina M. Artemieva[3], Ian D. Bastow[4], Fabio Cammarano[3], John R. Evans[5], Warren B. Hamilton[6], Bruce R. Julian[1], Michele Lustrino[7,8], Hans Thybo[3], Tatiana B. Yanovskaya[9]

[1]Dept. Earth Sciences, Durham University, Durham, U.K.

[2] Dept. Mathematics and Geosciences, University of Trieste, Italy and the Abdus Salam ICTP - SAND Group, Trieste, Italy & Inst. Geophysics, China Earthquake Administration, Beijing, China.

[3]Dept. Geography and Geology, University of Copenhagen, Denmark

[4] Dept. Earth Science and Engineering, Imperial College, London, SW7 2AZ, UK

[5]U.S. Geological Survey, Menlo Park, CA 94025, U.S.A.

[6]Dept. of Geophysics, Colorado School of Mines, Golden CO 80401, U.S.A.

[7] Dipartimento di Scienze della Terra, Università degli Studi di Roma La Sapienza, P.le A. Moro, 5, 00185, Rome, Italy

[8]CNR – Istituto di Geologia Ambientale e Geoingegneria (IGAG) c/o Dipartimento di Scienze della Terra, Università degli Studi di Roma La Sapienza, Rome, Italy

[9]Dept. Physics of the Earth, Sankt-Petersburg State University, Sankt-Petersburg, Russia

Non semper ea sunt quae videntur

Fabularum Phaedri - Liber Quartus – Fab.2

Abstract

Geological and geodynamic models of the mantle often rely on joint interpretations of published seismic tomography images and petrological/geochemical data. This approach tends to neglect the fundamental limitations of, and uncertainties in, seismic tomography results. These limitations and uncertainties involve theory, programming, correcting for the crust, the lack of rays throughout much of the mantle, the difficulty in obtaining the correct strength of anomalies, choice of what background model to subtract to reveal anomalies, and what cross-sections to select for publication. The aim of this paper is to provide a relatively non-technical review of the most important of these problems, collected together in a single paper, and presented in a form accessible to non-seismologists. Appreciation of these issues is essential if final geodynamical models are to be robust, and required by the scientific observations.

1 Introduction

Seismic tomography is the only tool available to map the deep structure of Earth, and it comprises a pivotal element of geochemical and dynamical models of the mantle. However, seismic tomography results are limited by issues that are not widely appreciated, in particular by non-seismologists. Counter-intuitively, teleseismic tomography cannot image the three-dimensional structure of the mantle. In all tomography methods, the strengths of calculated anomalies depend on subjective choices of inversion parameters, but are still commonly translated directly into critical geological parameters such as temperature and density. Tomography does not return thermal or geological information, but seismological parameters, and assumptions have to be used to translate seismic results into other physical parameters, *e.g.*, temperature or convective motion. Resolution- and error-assessment methods cannot encapsulate the true errors, and are insensitive to critical experimental limitations that invalidate parts of most derived structures.

Petrology and geochemistry are indirect tools for probing the mantle. They can provide information on its composition, but with virtually no spatial resolution. Isotope geochemistry can add a fourth dimension (time). The results from seismic tomography and petrology/geochemistry are frequently combined to develop geological models of the structure and dynamics of the mantle. This endeavor is, however, fraught with difficulties. Few practitioners are equally expert in both disciplines, and often the data from the more familiar discipline are interpreted jointly with published interpretations from the less familiar one. Critical appraisal of one discipline, combined with relatively little questioning of the other, runs the risk of unsafe interpretations. Tomography models are all too often assumed to provide essentially proof positive of things that the data physically cannot prove.

Here we provide an accessible overview, aimed primarily at non-seismologists, of the main problems that limit seismic tomography. This paper is not intended to be an in-depth, technical review for theoretical seismologists. That material can be found elsewhere (e.g., Aki and Richards, 2002, Dahlen and Tromp, 1998, Nolet, 2008). It is essential to appreciate the main problems inherent in many tomographic results published over the last four decades, but not

obvious *prima facie*, if cross-disciplinary interpretations are to be made that are both robust and required the data.

2 Methodological problems

2.1 Tomographic methods

Tomography methods used to image large-scale structures in the mantle may be grouped into three main classes: teleseismic-, surface-wave- and whole-mantle tomography. The first two are most sensitive to shallow mantle structure. The latter is the only method that can provide significant information about the lower mantle.

Teleseismic tomography uses the relative arrival times of seismic waves from distant earthquakes. It has resolution on the scale typically of tens of kilometers. The earliest technique of this kind is known as "ACH" (Aki-Christoffersson-Husebye, Aki et al., 1977, Christoffersson and Husebye, 2011). An array of seismic stations records a number of (often a few hundred) distant earthquakes (teleseisms) from various directions and distances. Differences, relative to reference models, in the arrival times of the seismic waves across the array are then used to determine the three-dimensional distribution of relative wave speeds beneath the array. The imaged volume typically extends down to a depth equivalent to the breadth of the surface array, which is commonly a few hundred kilometers. The method has been applied to a variety of geologic/tectonic settings, *e.g.*, volcanic regions, including Yellowstone, Iceland and Hawaii (Evans and Achauer, 1993, Foulger et al., 2001, Wolfe et al., 2009), continental rift zones (Achauer et al., 1992, Bastow et al., 2008, Bastow et al., 2005, Green et al., 1991), orogens and mountain ranges (Alinaghi et al., 2007, Lippitsch et al., 2003, Medhus et al., 2012, Paul et al., 2010), and cratonic regions (Gregersen et al., 2002, James et al., 2003, Obrebski et al., 2011, Rawlinson and Fishwick, 2012). The original experimental design, developed when computer resources were limited, was subsequently improved and alternative methods tried by many authors (e.g., Dahlen et al., 2000, Menke, 1984, Nolet, 1985, Paige and Saunders, 1982). The basic method has remained fundamentally the same, however, and as a result, its shortcomings persist.

Surface-wave tomography (Cara, 1979, Woodhouse and Dziewonski, 1984) utilizes waves whose energy is concentrated near the surface. Dispersion, caused by the dependence of surface-wave speed on the depth range sampled by each wavelength, provides information on wave speeds over a relatively broad depth range. Inversions for v_S structure tend to emphasize the stability and resolving power of the solution rather than smoothness (*i.e.*, the strength of wave-speed contrasts) (Backus and Gilbert, 1967, Backus and Gilbert, 1968), and Backus‑Gilbert averaging kernels ("resolution functions") provide the information critical for meaningful interpretation of the results. Many regional (e.g., Bruneton et al., 2004, Darbyshire, 2005, Lebedev et al., 2009, Simons et al., 1999, Van Der Lee and Nolet, 1997) and global (e.g., Billien et al., 2000, Dziewonski, 1971, Dziewonski, 1971, Ekström et al., 1997, Panza et al., 2007, Shapiro and Ritzwoller, 2002, Trampert and Woodhouse, 1995) surface-wave tomography models are now available. An important target is upper mantle radial anisotropy, which results from the different speeds of horizontally (SH) and vertically polarized (SV) shear waves and horizontally and vertically propagating P waves (Anderson, 1965, Gung et al., 2003, Kustowski et al., 2008, Lévêque et al., 1998, Marone et al., 2007, Tanimoto and Anderson, 1984).

Whole-mantle tomography, as its name implies, deals with the entire mantle. As a result, the earthquakes used are within the study volume instead of outside of it, as is the case with teleseismic tomography and much surface-wave tomography. Because of this, it is free of some, but not all, of the difficulties that we discuss below.

2.2 Structure outside the study volume cannot be ignored

In teleseismic and surface-wave tomography, attributing arrival-time anomalies entirely to local structure is equivalent to assuming that the structure outside the study volume is strictly one-dimensional (laterally homogeneous) and corresponds exactly to a "standard" Earth model. In reality, mantle heterogeneity is pervasively strong and three-dimensional, so that structure outside the study volume significantly affects observed arrival times. The contaminating effect of outside structure is mathematically of the same order as the effect of structure within the study volume (Julian and Foulger, 2013) and furthermore, numerical experiments using three-dimensional whole-mantle models show that these effects are of comparable magnitude ((Julian and Foulger, 2013, Masson and Trampert, 1997).

In teleseismic tomography, the biasing effects of external structure can be reduced by treating the shapes and orientations of incident wave fronts as unknowns and solving for them during tomographic inversion (Julian and Foulger, 2013). If a plane-wave approximation is used, the forward problem turns out to be particularly simple: the change in arrival time at a seismometer is the same as the change at the original entry point of a ray into the study volume. It is not necessary to determine the change in the ray path. Whole-mantle and local-earthquake tomography methods use an equivalent approach, solving simultaneously for the locations and origin times of earthquakes and for structure (Thurber, 1993). Each earthquake adds four unknowns to the problem (three spatial co-ordinates, plus the event origin time), but the resulting matrices are sparse and special numerical methods can reduce the computational burden (Spencer and Gubbins, 1980). Using plane wavefronts in the distant-source problem is even simpler, because, each event adds only three unknowns to the problem. Application of this potential improvement to existing data sets has not yet been done, but it may produce significantly better results than earlier studies, which used only a single, simple wavefront per earthquake. In surface-wave tomography, analogous corrections are possible (Yanovskaya, 2009).

2.3 The three-dimensional structure of the target volume is not retrieved

Contrary to popular assumption, and surprisingly, teleseismic tomography does not retrieve the three-dimensional structure of the study volume. The estimates of wave speed variations are, for each layer, *relative to that layer's average*. The absolute values of those averages remain unknown (Aki, et al., 1977). Two problems result from this (Léveque and Masson, 1999):

1. Wave speed variations are known only in the horizontal directions. Variations in the vertical direction are not calculable. These are removed entirely during computation of the relative arrival-times. While one may infer that a vertically arrayed set of anomalies represents a through-going structure, this is a weak inference that cannot be proven and is rendered even more suspect by the high-angle smearing inherent in teleseismic tomography (Section 2.7 and Appendix 1);

2. Negative anomalies are often interpreted as absolute low wave speeds whereas they may, in truth, be absolute high wave speeds if the average value of the layer is anomalously

high. Similarly, positive anomalies cannot be assumed to represent absolute high wave speeds.

Difficulties in resolving the depth extent of anomalies are exacerbated by the smearing problem, that causes anomalies to be elongated along ray bundles (Appendix 1). In the case of teleseismic tomography, these are primarily steeply dipping, and the result is artificially vertically elongated anomalies (Figure 1). The addition of waves from local sources may improve the vertical resolution. This approach works best in seismically active areas but, in principle, man-made sources also may be used. Such an approach may be economically unrealistic, however, and the frequency content will be substantially different between the teleseismic and local arrivals. Nevertheless, long range, controlled source experiments targeting the crust and mantle may complement the teleseismic method and lead to improvement in resolution of the vertical velocity changes. As such, teleseisms and local earthquakes should be integrated, wherever feasible (Evans and Zucca, 1993, Julian and Foulger, 2013).

Surface-wave tomography suffers from a different set of problems. Depth resolution depends critically on the wave period and the number of higher-mode waveforms used and frequency resolution. Fundamental modes sample only the crust and uppermost layers of the mantle (Figure 2a) (Ritsema et al., 2004). Although long-period Rayleigh waves and higher modes penetrate deeper, in practice, depth resolution tends to be low (Knopoff and Panza, 1977). In the uppermost mantle, wave-speed variations within a depth range of 30–50 km are indistinguishable, when only long-period waves are used, and nominal depths given for both horizontal and vertical and cross-sections refer to a broad, often at least 50 km thick, depth interval over which wave-speed structure is integrated (Figure 2c) (Ritsema, et al., 2004). This problem is worse for teleseismic- and whole-mantle tomography, where depth averaging often involves an even thicker interval. The resolution of surface-wave tomography is worst for the depth range ~300–400 km which is, inconveniently, the depth to which the deepest roots of cratonic lithosphere extend (Polet and Anderson, 1995). Including overtone waveforms is useful to enhance resolution in the transition zone (Li and Romanowicz, 1996, Ritsema, et al., 2004). However, interpretation of these data remains difficult and requires apposite weighting schemes with the dominating fundamental-mode branches (e.g., Ritsema, et al., 2004). As a result, available global models are characterized by low structural similarity in the transition zone at

long wavelengths (Cammarano et al., 2011) (Figure 3).

It is nevertheless clear from surface-wave studies that the upper 200 km of the mantle is a very heterogeneous and anisotropic region. Total travel-time delays in this region are similar to crustal delays. This region is often neglected, or modeled only simply with station corrections, in teleseismic travel-time studies (e.g., Montelli et al., 2004) but its affects may influence conclusions about the structure of the deeper mantle.

2.4 Correcting for the crust

All seismic stations are deployed at the surface. Thus, in order to extract the structure of the mantle, correction must be applied for the crust and for any part of the shallow mantle that is unresolvable because there are no crossing rays. In the case of teleseismic tomography, one approach is to solve for a correction for each seismic station ("station corrections" or "station terms"). Alternatively, a crustal model can be used. An example is CRUST 2.0 (Bassin et al., 2000), which specifies crustal structure on a 2˚ x 2˚ grid (~ 225 x 225 km). Older tomographic inversions may have used earlier, coarser models, *e.g.*, CRUST 5.1 (Mooney et al., 1998), which averages crustal structure over 5˚x 5˚ blocks (~ 560 x 560 km). However, the resolution of crustal models is highly variable, and is usually much worse than 500 km except for small, local areas.

These corrections may amount to as much as half of the entire travel-time delay, and they may even exceed the delays associated with structures imaged at depth and interpreted as bodies of primary significance. For example, in the teleseismic tomography study of Hawaii by Wolfe et al. (2009), the range of station corrections across the network was ~ ± 3 s, whereas the residual *S*-wave arrival-time anomalies, after correction had been made, which were used to image deeper structure, only amounted to ~ 2-3 s. In addition to the crustal effect, the 200-km-thick boundary layer underneath can have an equally large effect (Anderson, 2011). A way to overcome this problem is to obtain the local crustal structure by carrying out a densely spaced, controlled-source seismic program in combination with a receiver function study for the seismic stations of the array.

The problem of correcting for the crust also affects surface-wave- and whole-mantle

tomography. If inadequately done, corrections based on hypothetical crustal structure can erroneously propagate into images of mantle structure. For example, the PREM whole-mantle model (Dziewonski and Anderson, 1981), often used as a starting model, includes a 21.4 km-thick globally averaged crust. This differs significantly from both the true oceanic and continental crust. As a result, structural artifacts can appear at tectonic boundaries (Boschi and Ekstrom, 2002, Panning et al., 2010, Ritsema, et al., 2004). To minimize these problems, crustal corrections may be incorporated into inversion (Legendre et al., 2012).

For the longest-wavelength (> 200 s) Rayleigh-waves, the crustal effect is relatively small (Figure 4) (Mooney, et al., 1998, Ritsema, et al., 2004). These waves average the entire upper mantle and are insensitive to lithospheric structure (Figure 2a) (Ritsema, et al., 2004). For waves with shorter periods, however, the problem may be greater. For periods of 150 s, the crustal contribution may reach 50% of the total wave-speed variations calculated. For 40 s Rayleigh waves the contribution may be 100% (Artemieva, 2011, Ritsema, et al., 2004). Heterogeneities such as large sedimentary basins or calderas may have a significant effect. For Rayleigh waves with periods of 35 s, an error in estimated basin thickness of only 1 km may produce a 1% error in mantle phase wave-speeds (Bassin, et al., 2000). Low-density ice sheets also have strong effects, in particular at short and intermediate periods (Figure 4) (Ritzwoller, et al., 2001). In such situations, direct geological interpretation of surface-wave phase or group velocity tomography maps may not be possible. Crustal corrections play an even larger role for determining radial anisotropy structure (Panning, et al., 2010).

2.5 Anomaly amplitudes cannot be reliably determined

Anomaly amplitudes calculated using all tomographic methods are heavily dependent on relatively arbitrary aspects of the inversion process (Song and Helmberger, 2007). Figure 5 shows, for example, different teleseismic tomography models for mantle structure at 165 km beneath Ireland (O'Donnell et al., 2011). The rightmost upper two models achieve essentially the same goodness of fit to the data (*i.e.*, RMS data misfit reduction, shown on the vertical axis of the graph lowermost). Nevertheless, the amplitudes of the anomalies obtained are radically different.

The amplitudes calculated can be varied at will or unknowingly, by changing inversion program input parameters in ways that do not materially affect the data fit. Factors may include weightings of the different datasets included in the inversion, choice of damping factors and model smoothness, and the mathematical way in which the study volume is described, *e.g.*, whether uniform blocks or wave-speed gradients between grid points are used. In addition, the depth to the base of the study volume must be chosen, whether or not to use station corrections and how to correct for the crust. Synthetic tests can rarely reproduce the amplitudes of velocity perturbations in input models (Figure 1) (Christoffersson and Husebye, 2011, Eken et al., 2008).

The tomographic inversion problem is inherently and always underdetermined, i.e. there are fewer data than model unknowns. Thus it is impossible to find a unique solution. This problem is typically addressed by adopting a "regularization" scheme (Trampert and Spetzler, 2006). A final model is chosen that most closely matches the initial model estimate (e.g., Aki, et al., 1977, Tarantola, 1987), for example by damping the amplitudes of anomalies with respect to the starting one-dimensional velocity model (e.g., Evans and Achauer, 1993). Alternatively, the chosen model may contain the least amount of roughness in the structure required to explain the data (e.g., Constable et al., 1987, VanDecar, 1991).

For both approaches, a trade-off curve provides a selection of models to choose from, but deciding precisely which model is best is somewhat ad hoc and does not deal with the limits imposed by choices of parameterization. Sometimes the knee of the trade-off curve is preferred, and sometimes *a priori* estimates of data error govern the final choice (Figure 4 from the study of O'Donnell, et al., 2011). The *a priori* constraints, damping and smoothing, control resolution of the result (Debayle et al., 2005, Kustowski, et al., 2008, Lebedev and Hilst, 2008, Legendre, et al., 2012, Zhou et al., 2006). The nature of the resulting images, in particular the amplitudes, varies considerably as the damping parameter is varied. In most tomographic studies, model dependence on regularization levels is not displayed, so the information required to judge the reliability of the chosen image is not available.

Choices of final models are often made on the basis of residual travel-time anomaly vs. model roughness and estimated from trade-off curves () (O'Donnell, et al., 2011). However, the value chosen may simply be the one at the steepest point of the curve, chosen on the basis of some

estimated data error, or simply the value that gives the result that fits best geological models assumed at the outset to be correct (Foulger, et al., 2001). Such an approach erodes the hypothesis-testing power of the work. It is popular to apply the principle of Occam's razor to select smoothly varying models (e.g., Boyadzhiev et al., 2008). This, however, only guarantees that the wave-speed amplitudes will be underestimated. Smoothing is achieved using the average of adjacent blocks, and it works to suppress the amplitudes of small, high-gradient features (Figure 6). A further disadvantage of this is that blocks containing no rays are interpolated or extrapolated to the grid edges, producing wave-speed perturbations in regions that may contain no data. Smoothing can also be achieved at the plotting stage by interpolating the wave speeds between homogenous blocks and using a continuous color spectrum, or more physically by something like an offset-and-average technique (Evans and Zucca, 1993).

Low-amplitude damping, which permits models with large wave-speed perturbations, has a different effect and creates a patchy image. When a tomographic model contains many under-sampled blocks, this method can produce solutions with spurious small-scale velocity anomalies, compared to the size of the blocks. Where a strong contrast really does exist in the seismic structure, *e.g.*, at the ocean/continent edge, damping will not reproduce either true structure, and will underestimate the true velocity variations (Kennett, 2006). It is possible to assess the degree of smoothing incurred by the tomographic inversion by inverting synthetic traveltimes for known theoretical models, and to some degree estimate the possible range of real velocity anomalies (Alinaghi, et al., 2007). This approach has been applied to crustal studies with controlled sources (e.g., Nielsen and Thybo, 2009).

True amplitudes can be distorted in surface-wave tomography by limited lateral resolution (Figure 2c) (Ritsema, et al., 2004). At 150 km depth beneath Australia, for example, lateral resolution of the S20RTS surface-wave model (Ritsema et al., 1999) is almost half the continent in width, and includes oceanic, Archean and Proterozoic provinces. The problems in amplitude resolution are revealed when independent groups perform inversions using similar datasets, and obtain very different anomaly amplitudes. An example is inversions for the structure of the Western U.S.A. mantle, using USArray data (Becker, 2012, Sun and Helmberger, 2011).

Efforts have been made in recent years to improve anomaly amplitude recovery using various approaches. However, the inherently under-determined nature of tomographic inversions means that some form of regularization (e.g., damping or smoothing) is invariably required. Thus, there is likely to always remain an inherent problem with true amplitude recovery using seismic tomography.

2.6 Inhomogeneous ray coverage

Earth's mantle is not uniformly sampled by seismic waves. Earthquakes are concentrated in narrow belts, and most are shallow, *i.e.*, in the upper few hundred kilometers. Only in a few regions do they occur as deep as the transition-zone. Very few occur beneath the 670-km discontinuity (Anderson, 1967, Anderson, 2007, Hamilton, 2007). All seismic stations are deployed at Earth's surface, mostly on land, with very few on the sea floor. As a result, the distribution of measurable seismic rays in the mantle is extremely non-uniform, and so also is the resolution of tomographic models. The situation is improved by the use of many different phases, *e.g.*, surface waves and core-reflected waves, but even so, much of the mantle is poorly sampled (Figure 7).

This problem leads to two major difficulties that affect all tomography methods:

1. The structure of much of the mantle is essentially unobtainable. In inversions, wave speeds in these regions are not significantly perturbed from the hypothetical starting model. Unfortunately, most color illustrations of tomographic images do not distinguish between regions where the wave speed is confidently determined to be the same as the starting value, and regions where the starting value is retained because of lack of data (Section 4). Apparent anomalies in the resulting images may thus correspond to those volumes where seismic rays exist, because only there can inversions change the initial starting value. Some apparently compact anomalies may simply be sampled portions of much wider anomalous regions.

2. Some regions may be heavily sampled by rays, but these may comprise quasi-parallel bundles, with few crossing rays. An example of this problem from teleseismic tomography is a study done at Hawaii, where a deep, low-wave speed anomaly

interpreted as a plume is dependent only on steeply upcoming SKS waves (waves that pass through the core; right panel, Figure 8). This ray bundle is approximately colinear to the body illustrated, but could equally well be explained by structure outside the study volume or at shallower depth, somewhere along the ray-bundle path. The systematic and non-uniform configuration of sampling rays in the Hawaii region renders teleseismic tomography ineffective there for imaging below the base of the upper mantle (Cao et al., 2011, Li et al., 2008).

The Hawaii region is perhaps the worst-located in the world for teleseismic tomography. It is essentially equidistant from most parts of the distant, circum- , seismogenic plate boundaries. Usable earthquakes thus tend to have similar epicentral distances and angles of approach and arrive beneath Hawaii with a skirt-like distribution. The landmass is relatively small (the Big Island has a maximum diameter of only ~150 km) and the travel-time corrections necessary for the exceptionally thick igneous crust and lithosphere are greater than some associated with underlying mantle anomalies for which significance is claimed (Section 2.4). The mantle throughout the Pacific has exceptionally low wave speeds compared with the global average, complicating the choice of an appropriate *a priori* model (Gu et al., 2001).

Inhomogeneous sampling is a major problem in whole-mantle tomography. Figure 9 shows images interpreted as deep-mantle plumes beneath various ocean islands (Montelli et al., 2006, Montelli, et al., 2004). These “anomalies” are likely artifacts of quasi-parallel, upward-traveling ray bundles recorded on island seismic stations that are surrounded by large oceanic regions devoid of stations, and thus of recorded seismic waves. As a result, a one-to-one correspondence between observed “plume-like” anomalies and ocean-island seismic stations was produced (van der Hilst and de Hoop, 2005). Similar problems can arise in the case of sparse continental networks. The problem is particularly acute for whole-mantle tomography models that are parameterized using spherical harmonics. Using this computational approach, resolved anomalies or simply noise may be mapped into regions where there are no rays whatsoever. In the case of surface-wave tomography, linear “artifact anomalies” appear in tomography models along the dominant, horizontal ray directions (Figure 10) (Feng et al., 2007, van der Lee et al., 2001).

2.7 Resolution and checkerboard tests: Perils and pitfalls

Teleseismic tomography is valid at most to a depth about equal to the aperture of the observational array, and then only when the ray set used is uniformly distributed in location and orientation. Both measures of ray homogeneity apply individually at every location in the modeled volume and affect neighboring volumes. Deeper and peripheral features in the inversion result are in all cases unreliable and should not be interpreted. While this information is encapsulated in the columns of the inversion resolution matrix (**R**) or its equivalent (individual resolution tests for single-block anomalies), many other problems are not expressed in the mathematics or numerical results. Checkerboard tests of **R** are effectively meaningless. They are optimal for damped inverses (because kernels of **R** have negative side lobes and reinforce alternating high-low wave speed patterns) and are thus optimistic and misleading (Léveque et al., 1993, van der Hilst et al., 1993) (Appendix 1).

Cryptic problems derive from the approximations, parameterization, damping, linearization, and finiteness of the ray set used. In short, they derive from the numerous differences between the true Earth structure and its approximation by all types of tomography. In addition, current methods of measuring seismic travel times (VanDecar and Crosson, 1990) subsume systematic errors that then map into calculated models and are effectively impossible to quantify or to recognize in the results.

The common failure to understand and deal with these problems has led to a number of unsupportable claims of deep, narrow wave-speed anomalies interpreted as plumes extending well into the lower mantle, and even as far as the core-mantle boundary (Bijwaard and Spakman, 1999, Montelli, et al., 2006, Montelli, et al., 2004, Montelli et al., 2004, Wolfe et al., 2011, Yuan and Dueker, 2005). While teleseismic tomography cannot eliminate the possibility that such anomalies exist, neither can it confirm them or provide relevant constraints. The only test we are aware of that can demonstrate the presence of deep, low-wave speed conduits is by using steep rays to search for guided waves–so-called “fiber optic” modes (Julian and Evans, 2010). While this test could be attempted with several existing data sets, it has not, to our knowledge, so far been done.

Lack of consideration of resolution leads to anomalies that are too small or too weak to have been resolved (*i.e.*, noise or artifact) being presented in published images and interpreted. This can lead to the use of unreliable tomographic images as support for assumptions, rather than to the use of reliable features to test hypotheses. An example is the widespread use of unresolved images to bolster the concept that volcanic areas are fed by hot, rising diapirs. Alternative, shallow-based models to explain migrating- and large-volume volcanic systems have been suggested, such as water in the mantle near ridges or transform faults (Bonatti, 1990), shear heating at the base of the lithosphere (Anderson, 2011, Doglioni et al., 2005, Shaw, 1973), the effect of adjacent glaciers (Carminati and Doglioni, 2010) or instabilities produced by cold down-welling material (Davies and Bunge, 2006). These mechanisms do not require deep-seated seismic anomalies, and if they are to be tested, only those anomalies that are really required by the seismic data should be used.

A second example is the thickness of the cratonic LID. A number of studies that argue it is no thicker than 200-250 km (e.g., Gung, et al., 2003) need more conclusive evidence (Artemieva, 2011). Models based on fundamental surface-wave modes lose resolution at 200-300 km depth (Figure 2). Even when higher overtones are included, resolution is weakest at 300-400 km. Vertical structure cannot be resolved better than 30-50 km, and vertical averaging occurs over several tens of kilometers. Limitations in lateral resolution, in particular for global or continent-scale models, lead to spatial averaging across tectonic provinces with significantly different lithospheric structure (Kennett, 2006). In western Australia, the Archean cratons are located in a poorly resolved region (Simons, et al., 1999). As a consequence, the relatively thin LID (~200 km) proposed on the basis of data collected on the SKIPPY seismic stations of the Australian National Universities (http://www.ga.gov.au/meta/ANZCW0703003617.html) may be an artifact of poor model resolution.

2.8 Repeatability

If a feature imaged by tomography is reliable, it should be resolvable in multiple independent studies. Geological significance should only be attributed to features detected in all reputable studies (Foulger et al., 1995, Shapiro and Ritzwoller, 2002). illustrates this problem at Hawaii. There, two independent studies both resolved a strong, low-wave speed anomaly in the upper

few hundred kilometers of the mantle (Li, et al., 2008, Wolfe, et al., 2009). This part of the two images may be considered reliable, at least in location and sign. On the other hand, the trajectory of downward-continuing low wave speeds into the lower mantle are almost exact mirror images in the two studies. These bodies, and even the very existence of a downward continuation of the shallow, low-wave-speed anomaly, are unreliable.

Tomographic models of the purported whole-mantle-crossing "Farallon slab" are shown in Figure 11. This structure is frequently cited as the strongest evidence available for the sinking of slabs to the core-mantle boundary (e.g., Kellogg and Wasserburg, 1990). Nevertheless, the shape of the lower-mantle, high wave speed anomaly is very different between different results. It is a feature of global extent, too large to be explained as a single subducted slab, in particular when slab thermal- and compositional re-equilibrium with the mantle are considered. The true extent and geological nature of much of this anomaly thus remains uncertain.

Only in a few cases have formal uncertainties in tomographic results been published in papers (e.g., Brandmayr et al., 2010, Corchete and Chourak, 2010, Corchete and Chourak, 2011, Gonzales et al., 2011, Panza, et al., 2007, Raykova and Panza, 2010). If uncertainties were published routinely, many seismic anomalies interpreted geologically, widely used in undergraduate teaching, and relied upon to support geochemical and geodynamic models, would be recognized as noise or artifacts (Shapiro and Ritzwoller, 2002).

3 Absolute and relative wave speeds

Teleseismic tomography retrieves only *relative* wave speeds. There are no ray turning points (i.e., where the rays change from a downward to an upward trajectory) within the target volume, the method cannot recover absolute wave speeds, and the mean anomaly of the final result is constrained to be zero relative to the reference model. These facts profoundly influence how the results are typically illustrated and, as a result, interpreted.

Illustrations commonly comprise color maps and cross sections showing either the relative anomalies as percent deviation from the original starting model, or absolute wave speeds determined by adding the relative anomalies back into the starting model. It is critical to

understand a number of issues with these illustrative approaches if the results are to be understood correctly, even where they are well-constrained.

3.1 Interpreting relative anomalies

Color plots typically show positive (fast) and negative (slow) anomalies relative to a "zero" contour that corresponds approximately to the mean wave speed in each individual layer (Bastow, 2012). Such a plot is *constrained* to contain approximately equal volumes of positive and negative anomalies.

This illustration style encourages the perception that the positive and negative anomalies are relative to some global average. Such a perception is almost always wrong. Figure 12 shows the global tomographic model of Ritsema et al. (2011) compared with two regional tomographic studies, one from Canada (Frederiksen et al., 2007) and the other from Ethiopia (Bastow, et al., 2008). The "zero contours" in the two regions clearly correspond to radically different absolute wave speeds. In the case of the Canada study (left), the average wave speed relative to a global mean (middle) is high. The opposite applies to the Ethiopia study. There, relative to the global mean, wave speeds in the region are extremely low–as much as 6% low, and amongst the lowest for any continental area (Bastow, et al., 2008, Bastow, et al., 2005). Despite appearances, white regions are not "normal" compared to the global mean, and blue/red regions are not anomalously fast/slow. This problem can propagate into physical interpretations, by encouraging interpretation in terms of physical properties that are low or high relative to a global average, *e.g.*, temperature.

Different interpretations of relative arrival-time tomographic images have, for example, resulted in markedly different tectonic interpretations of tomographic studies in Ireland and the British Isles. Arrowsmith et al. (2005) suggested that absolute delay times in the UK are late with respect to the global mean, and interpreted low velocity anomalies as evidence for elevated mantle temperatures beneath the region. Wawerzinek et al. (2008) drew similar conclusions for the Irish mantle. In contrast, O'Donnell et al. (2011) cited evidence from global (Ritsema, et al., 2011) and regional surface wave models (measures of absolute wave-speed; e.g., Pilidou et al., 2004, Pilidou et al., 2005), and more recent catalogs of absolute travel-time delays (Amaru et al., 2008) to suggest that the background mean wave-speed in the UK/Ireland is, in fact, fast

compared to the global mean, precluding the need for a high temperature, partial-melt hypothesis to explain wave-speed variations beneath the region.

Relative wave-speed plots impart radically different visual impressions from absolute wave speed plots, which depict true Earth seismic structure (Section 3.2). Figure 13 compares an absolute global wave-speed model (bottom) with wave-speed perturbations relative to the background model used (middle). The most significant and reliable features are not visible in the relative model, including the global, upper-mantle LVZ (Thybo, 2006). Similar plots for southern Africa are shown in Figure 14, and for Siberia in Figure 15.

3.2 Interpreting absolute wave speeds

Absolute wave speeds are derived by adding the relative anomaly results to some "average" seismic model. Thus, the choice of model is highly influential. Figure 14 shows cross sections of southern Africa in the form of a) absolute wave speeds, and b-c) anomalies relative to two different global seismic models. Although careful inspection reveals common features between the three cross sections, at first glance they look radically different and there is clearly risk of misinterpretation. This risk would be higher if only one cross section were published, and even higher if the reference wave-speed model were not provided in a form that facilitates comparison with the cross section.

But which "average" wave-speed model should be used? Reference models such as PREM (Dziewonski and Anderson, 1981) or AK135 (Kennett et al., 1995) are not unique and depend on the data used to derive them. Since oceans comprise 70% of Earth, PREM is dominated by oceanic structure. Upper-mantle seismic wave-speed structure differs substantially between the oceans and continents, so a single, averaged global model is inappropriate for almost every region.

PREM has an abrupt increase in v_P and v_S at 220 km depth (the Lehmann discontinuity). Gu et al. (2001) conclude that it is found preferentially under continents, and is not global. Recent, three-dimensional models of v_S show that what is expressed as a step in PREM may be a rapid decrease in lateral heterogeneity between 200 and 300 km (Cammarano and Romanowicz, 2007, Deuss, 2009, Kustowski, et al., 2008, Thybo, 2006, Thybo and Perchuc, 1997). This feature is

not necessarily global, however. The Lehmann discontinuity is, nevertheless, inherited by all tomographic models that are calculated using PREM as a starting model. Smoothing PREM does not entirely solve this problem but results in perturbed seismic wave speeds in a zone ~ 140 km thick centred at 220 km depth that do not reflect true Earth structure (). Many stable continental regions contain positive wave-speed anomalies as deep as 300 km, and thus the wave-speed reductions and strong gradients commonly observed in derived models at ~220 km depth may be artefacts. Further discussion of this may be found in Thybo (2006).

Because PREM is used in this way, many authors have concluded from inversion results that in stable continental regions the lithosphere-asthenosphere boundary is at ~220 km depth. In truth, calculating such a feature at this depth was made inevitable by the original starting model used. Inclusion of any sharp wave-speed discontinuity in the starting model will lead to an inversion result with high/low wave speeds above/below the discontinuity, simply because the tomography result is a smoothed version of the starting model (). In addition, it should be noted that the lithosphere/asthenosphere boundary is a rheological, and not a seismic, boundary.

The question of what is an appropriate reference model is particularly important in the case of subduction zones. If the starting model LVZ wave speeds are too high, the imaged slab will appear to be broken. Artificial slab detachments appear in images of the Apennine, Zagros, Hellenides, Andine, and Farallon slabs. Tomographic cross-sections of the Aegean typically reveal a false discontinuity in the slab at 100-150 km depth (Agostini et al., 2010). Displaying tomographic results for the Mediterranean region is problematic because of strong lateral heterogeneity there. A study volume may contain both continental and oceanic subducted lithosphere because a complex of passive continental margins inherited from the Tethys Ocean was subducted (e.g., Carminati et al., 2012, Handy et al., 2010). Some subducted material may even have wave speeds lower than those of the hosting mantle. Under these conditions, realistic geologic structure cannot be illustrated using a single one-dimensional reference model, and three-dimensional starting models need to be used. Misleading images parse into interpretations, *e.g.*, in the apparent misalignment between shallow, subduction-related earthquakes and the high-wave-speed zone inferred to be the subducted slab (Agostini, et al., 2010).

Methods do nevertheless exist for retrieving absolute wave speeds, and not just perturbations to a starting model (e.g., Cammarano et al., 2003, Katzman et al., 1998, Levshin et al., 2007, Panza et al., 2010, Ritzwoller et al., 2002, Shapiro and Ritzwoller, 2002, Thybo, 2006, Yang et al., 2007, Yanovskaya and Kozhevnikov, 2003; http://ciei.colorado.edu/~nshapiro/MODEL/). The best absolute models use all available data, including, for example, local and regional earthquakes and man-made sources, which introduce turning waves (e.g., Anderson, 2011, Brandmayr et al., 2011, Du and Panza, 1999, Panza, et al., 2007). These are superior to models based on adding calculated anomalies to starting models.

4 Displaying the results

Published tomographic maps and cross sections may give very different impressions, depending on the design choices made, and there is wide scope for designing figures that support preferred geological theories:

1. Regions where there are no sampling rays are commonly filled with the "zero anomaly" color corresponding to no perturbation to the initial starting model. They are thus indistinguishable from well-sampled regions where a wave speed similar to the initial model was robustly determined (Section 2.6). Such use of color can give the visual impression that an anomalous region, well-resolved because it lies beneath the center of the network, is embedded in extensive volumes of "normal" background structure;

2. Vertical exaggeration can make short, broad bodies appear to be tall and chimney-like (Figure 16);

3. Where bodies are complex and three-dimensional, cross sections varying in orientation by only a few degrees, or by short distances laterally, can give very different visual impressions. Truncation of cross sections can conceal adjacent anomalies at odds with the preferred interpretation (Figure 17);

4. Very different impressions may be given, depending on the choice of color scales, and by using different scales for different parts of the imaged volume. Anomalies imaged in the lower mantle are generally much weaker than those imaged in the upper mantle. Despite this, figures can be constructed that give the impression that structures of relatively

uniform strength traverse the entire mantle. This can be achieved by using a color scale that saturates at a fraction of the maximum upper-mantle wave speed anomaly (Figure 17), or by using different color scales for upper- and lower-mantle sections. An example of the latter is a recent study by Wolfe *et al.* (2009), where the color scale used saturates at ±4% for anomalies at a depth of 100 km, ±2% for anomalies at 300 and 400 km, and at ±1% for anomalies at 600, 900 and 1200 km. A cross-section using a color scale throughout that saturates near to the upper-mantle maximum anomalies reveals the true picture, which is that a weak downward-continuing "tail" underlies a distinct and much stronger shallow anomaly that does not extend deeper than 400-500 km (Figure 17, right). Saturating the color scale at very low anomaly amplitudes can also impart the visual impression of significance to anomalies that are simply noise, *i.e.*, too weak to be resolved.

There is some justification for varying the color scale with depth because the sensitivity of wave speed to some parameters of geological interest, *e.g.*, temperature, changes with depth (Julian, 2005). However, it is questionable practice to involve such considerations in primary, result-presentation figures. Furthermore, the anomaly illustrated in (right) cannot be explained by this effect alone. The weak "tail" overlaps in depth extent with the much stronger adjacent anomaly in the transition zone, and its contrast with the strong, shallow body is too great to be explained by depth-temperature dependence alone.

5 Translating the results to other physical variables

It is common interpretive practice to assume that red and blue colors (low- and high-wave speeds) correspond directly to "hot" and "cold" volumes (e.g., Faccenna and Beker, 2010, VanDecar et al., 1995). For example, low relative wave speeds beneath the British Isles have been used to argue for hot, partially molten plume material with a temperature anomaly of ~ 200˚C (Arrowsmith, et al., 2005, Wawerzinek, et al., 2008). Low relative wave speeds below ~ 200 km under the Siberian Craton () and other stable continents have been ascribed to hot asthenosphere (McKenzie and Priestley, 2008). Many such interpretations are inappropriate because the apparent low wave speeds are not low on a global scale (Section 3) (Amaru, et al., 2008, Pilidou, et al., 2004, Pilidou, et al., 2005, Poupinet, 1979, Poupinet et al., 2003). Also, in

particular for local- and regional-scale structures, ambiguity in the physical interpretation of anomalies is commonly ignored, even in geologically complex areas. The amplitudes of seismic anomalies in published teleseismic tomography maps and cross-sections cannot be used meaningfully to constrain geological models or to estimate temperature, composition or degree of partial melt. This is because calculated amplitudes are largely subjective (Section 2.5).

Long-wavelength variations in global upper-mantle seismic models are mostly due to temperature (Cammarano, et al., 2011). However, on local and regional scales, mineralogical and chemical heterogeneities, as well as partial melt, crystal size, and the presence of hydrogen and carbon may have greater effects than temperature on seismic wave speed, and cannot be ignored (Table 1). The presence of melt strongly lowers wave speed (Hier-Majumder and Courtier, 2011, Murase and Fukuyama, 1980, Murase and Kushiro, 1979, Schmeling, 1985). The wave speed reduction in v_P and v_S corresponding to a temperature increase of ~100˚C can equally well be caused by the presence of < 0.5% of partial melt, or very small, unconnected grain-boundary melt fractions (Faul and Jackson, 2007). A reduction of ~2% in the forsterite content [Mg/(Mg+Fe)] in mantle olivine can bring about similar wave-speed reductions (Artemieva, 2009, Cammarano, et al., 2011, Chen et al., 1996, Chen, 1996, Jordan, 1979). Nevertheless, even when no correlation is observed between heat flow and temperature calculated using teleseismic tomography anomalies, the latter are still commonly interpreted solely in terms of temperature (Faccenna and Beker, 2010, Goes et al., 2000). Sensitivity of seismic wave speed to temperature decreases with depth (Cammarano, et al., 2003), and in the lower mantle compositional and thermal effects on wave-speeds may, as a general rule, be similar (Cammarano, et al., 2003, Deschamps and Trampert, 2004, Karato and Karki, 2001).

Natural examples from Alpine-type ophiolitic remnants, as well as seismic discontinuities at various depths below continents (e.g., Rychert and Shearer, 2009, Thybo, 2006, Thybo et al., 2003) clearly indicate pervasive compositional, metamorphic, and even melting heterogeneity that must affect wave speeds. Teleseismic tomography studies typically measure only v_P and v_S, but given the difficulty of determining anomaly amplitude reliably (Section 2.5), it is generally not possible to deduce unambiguously the physical explanations for observed wave speed variations.

There are a few exceptions to this, however. The most notable is the Large Low-Shear Velocity Provinces (LLSVPs–also known as "superplumes"). These are two vast regions of low v_S in the lower mantle beneath much of the southern Pacific Ocean and the southern Atlantic Ocean-South Africa-southwest Indian Ocean. It is widely assumed that they owe their low wave speeds to high temperature, and popular geodynamic interpretations assume this (e.g., Courtillot et al., 2003). It was, however, widely argued (Kellogg et al., 1999, Kennett et al., 1998, Saltzer et al., 2001, van der Hilst and Karason, 1999) and later shown using normal modes, that they owe their low wave speeds to compositional variations and that they have relatively high densities and approximately normal temperatures (Ishii and Tromp, 2004, Trampert et al., 2004, Trampert and van der Hilst, 2005). They are thus not buoyant or rising. Van der Hilst (2004) and Trampert et al. (2004) have suggested that abundant iron in the lower mantle, not high temperature, may account for their low wave speeds. Kuo and Romanowicz (2002) have questioned the resolution of this result, and a different approach, based on geoneutrino fluxes measured above and some thousands of kilometers away from the LLSVPs, could shed further light on this problem (Sramek et al., in press).

A further example of a low-wave-speed body that is not hot underlies the Ontong Java Plateau, extending from the near-surface down to ~300 km depth with v_S up to 5% lower than the global average. A study of seismic *ScS* phases (shear waves reflected off the core) reveals that attenuation within the body is low compared with the rest of the Pacific mantle (Gomer and Okal, 2003). The combination of low-v_S and low attenuation rules out temperature alone as the cause of the anomaly and requires a high-viscosity, chemical interpretation (Klosko et al., 2001).

Corresponding examples of high-wave-speed materials that are not dense or sinking are harzburgite and clinopyroxene-poor lherzolite. These are buoyant because the Fe-Mg solid solution minerals olivine and pyroxene are Fe-poorer than primitive (*i.e.*, have not been subject to previous basaltic melt extraction) mantle compositions. A suite of global and regional studies has shown that, as a general rule, the effects of temperature and composition on buoyancy are comparable in the shallow continental mantle (Artemieva, 2007, Brandmayr, et al., 2011, Forte and Perry, 2000, Jordan, 1975, Kaban et al., 2003, Kelly et al., 2003, Tumanian et al., 2012). In the deep mantle, composition and not temperature dominates buoyancy (Trampert and van der Hilst, 2005).

6 Implications for the geochemical and geodynamic models of the mantle

Acceptance of non-unique interpretations of tomographic images has led to geological and geodynamic models that are not required by the data. These include proposals that the British Isles are underlain by hot plume material (e.g., Arrowsmith, et al., 2005, Wawerzinek, et al., 2008), that plumes underlie several islands in the Indian Ocean (Montelli, et al., 2004, Montelli, et al., 2004), that a plume feeding Hawaii is rooted variously to the NW, or the SE of the Big Island (Li, et al., 2008, Wolfe, et al., 2009), and that sodic alkaline-to-tholeiitic continental and oceanic mid-plate magmatism require thermal anomalies (Piromallo et al., 2008, Ritter et al., 2001). The assumption that low seismic wave speeds indicate hot material has led to proposals that sub-lithospheric channels up to thousands of kilometers long connect volcanic regions thought to have similar geochemical signatures (e.g., Duggen et al., 2009, Ebinger and Sleep, 1998, Gibson et al., 1995, Niu et al., 1999, Oyarzun, 1997, Piromallo, et al., 2008).

East African Rift volcanism has been widely attributed to the "African superplume", but less emphasis has been placed on the absence of volumetrically relevant igneous activity in southern Africa over the last 180 Ma. This is consistent with the LLSVPs not being hot (e.g., Bailey, 1992, Pik et al., 2006). The exotic magmas of the East African Rift system, including strongly SiO_2-undersaturated kamafugitic, melilititic-to-leucite-bearing potassic/ultrapotassic magmas and carbonatites, suggest a compositionally anomalous underlying shallow mantle (e.g., Bailey and Woolley, 2005, Boven et al., 1998, Eby et al., 2009, Furman, 2007, Muraveva and Senin, 2009, Rosenthal et al., 2009, Tappe et al., 2003). The sources feeding these small-volume and low-degree-melting volcanic rocks are likely to have K_2O-H_2O-CO_2-rich compositions and to be significantly distinct from the anhydrous, four-phase peridotitic assemblage generally assumed in interpretations of tomographic images. An explanation for the volcanism rooted in shallow source compositional heterogeneity is more likely than lower mantle temperature excess.

In addition to local studies, tomography images are widely used by geochemists to support geochemical models of the entire mantle. For the reasons discussed above, this is sometimes invalid. Conversely, evidence from geochemistry is often cited in support of interpretations of seismic tomography images. This is sometimes equally invalid because interpretations of geochemical data also suffer from serious problems and ambiguities.

It cannot safely be assumed that high-wave-speed parts of the core-mantle boundary region are "slab graveyards", and that the LLSVPs are hot and buoyant. Together, these two assumptions underpin whole-mantle convection models that attribute the geochemical signature of ocean-island basalts to the sweeping up of subducted crust in deep-mantle plumes. This, in turn, has bolstered models that attribute geochemical species such as high-$^{3}He/^{4}He$ to the deep lower mantle, and the view that the core-mantle boundary is the only mantle region where significant radiogenic growth can occur (e.g., ^{206}Pb from ^{238}U; Hofmann, 1988, Hofmann, 1997, Hofmann, 2003, White, 2010). Interestingly, the highest $^{3}He/^{4}He$ measured in terrestrial basalts (~50 times the atmospheric $^{3}He/^{4}He$ ratio; Stuart et al., 2003) are associated with extremely high $^{143}Nd/^{144}Nd$ (0.51284-0.5135) and low $^{87}Sr/^{86}Sr$ (0.7030-0.7039) isotopic ratios, as well as low-to-very-low incompatible element contents (e.g., La/Lu normalized to CI chondrite estimate <1; Jackson et al., 2010). All these features indicate a depleted, not an undegassed/primitive, mantle source for these magmas. This apparent paradox has been explained by the percolation of high-$^{3}He/^{4}He$, small-volume melts from the deepest mantle in a depleted peridotite matrix.

It has been surmised that the remaining 99% of the mantle is too cold relative to its solidus temperature to melt, or that it is homogenized by convection, and regions of daughter-isotope accumulation cannot exist within it (e.g., Cadoux et al., 2007). As a result, it has been suggested that the upper mantle can only produce melts at mid-ocean ridges by passive adiabatic upwelling, and that igneous rocks with major- and trace-element compositions different from normal mid-ocean ridge basalt (NMORB) involve a separate, deep-mantle source (Farnetani et al., 2012, Webber et al., 2013, White, 2010, Zhou and Dick, 2013).

The view that geochemistry provides definitive proof for deep-mantle upwellings has been debated for at least 30 years, and yet remains controversial. From a geochemical point of view, the isotopic compositions of all oceanic-island- and ridge basalts, as well as nearly all mid-plate continental basalts (away from active or fossil subduction zones) can be wrapped in a four-apex polyhedron whose end-members have been labeled HIMU (High-μ, where $\mu = {}^{238}U/^{204}Pb$ ratio), EMI (Enriched Mantle type I), EMII (Enriched Mantle type II) and DMM (Depleted MORB Mantle; Zindler and Hart, 1986). A fifth, very common component (FOZO = Focus Zone) shows intermediate Sr-Nd-Pb-Hf isotope characteristics (Hofmann, 2003, Stracke, 2012, Stracke et al., 2005, White, 2010).

Isotopic similarities of oceanic or continental mid-plate magmas to one or more of the first three geochemical end-members (HIMU, EMI and EMII) are commonly considered to be proof for a deep-mantle source origin (Hofmann, 2003, White, 2010). However, there is no geochemical or petrological requirement for given Sr-Nd-Pb-Hf-Os-O-He isotope characteristics to arise from deep mantle sources. A definitive geochemical-petrological model of how Earth's mantle works is still lacking. More than three decades of geochemical research into basaltic magmatism have, nevertheless, led to three generally accepted conclusions:

1. the radiogenic and stable isotopic ratios of mid-ocean ridge and mid-plate magmas can be explained only by invoking the presence of recycled crust and/or shallow lithospheric-mantle and/or reactive products between high-pressure melts and ambient mantle matrix;
2. the upper mantle is highly heterogeneous from crystal- to continental scales and therefore not vigorously mixed and stirred as commonly assumed, and
3. no unambiguous evidence for mass transfer from the Earth's core has been demonstrated (e.g., Anderson, 2011, Lustrino, 2011, Scherstén et al., 2004, Stracke, 2012, Stracke, et al., 2005).

Any tomographic image used to argue for hot or deep mantle sources cannot, therefore, find support in geochemical observations. Geochemistry has no more ability than seismology to infer hot or deep sources for surface lavas.

The main debate in the geochemical and petrological community concerns the rheological properties of upper- and lower-mantle rocks. Of particular interest is the location where non-peridotitic lithologies (metasomatomes, or metasomatic layers) are isolated, allowing them to evolve peculiar high- or low isotopic ratios. In the framework of a vigorously and efficiently stirred mantle, the only volume escaping homogenization is the deepest mantle at D" (Hofmann, 2003, Stracke, 2012, White, 2010). In more realistic, heterogeneous mantle structures, non-convecting volumes are located in the shallow mantle (e.g., Anderson, 2011, Guarino et al., in press, Lustrino, 2011).

The chemical compositions of mantle sources cannot be deduced from the major- and trace-element contents of OIBs. Nevertheless, these contents do indicate fertile, enriched sources. This contrasts with evidence from Sr and Nd isotopic ratios that indicate many OIBs arise from

depleted, though non-primitive sources. The ^{3}He-poor composition of OIBs (typically $<10^{-11}$ cm^3 g^{-1}) compared with the ^{3}He-rich MORBs (typically $>10^{-11}$ cm^3 g^{-1}), is another indication that OIB sources are not primitive, as many geochemical models assume.

There are, nevertheless, examples where seismic and petrological data do comprise a useful mutual-support pair. A steep decrease in the carbonated peridotite solidus of 400-500 ˚C occurs at ~2 GPa (~60 km), approximately coinciding with the top of the LVZ under oceans. This suggests that layer contains partial melt (e.g., Presnall and Gudmundsson, 2011, Wyllie, 1988). The top of the LVZ also corresponds to the depth at which the pargasitic amphibole, the main water-storage mineral in the shallow mantle at average geotherms, becomes unstable. At this depth (~90-110 km), the water-storage capacity of mantle peridotite drops from ~0.3-0.4 wt% to a few hundred ppm (Green et al., 2010, Mierdel et al., 2007). As a result partial melting of lithospheric mantle may onset at the wet solidus (Thybo and Perchuc, 1997), several hundred degrees C cooler than the water-undersaturated solidus (Green, et al., 2010). The presence of small amounts of hydrous basaltic melts at these depths is also in agreement with the enhanced electric conductivity of the LVZ (Ádám and Panza, 1989, Ni et al., 2011).

7 Summary

The limitations of travel-time tomography include inadequate correction for structure outside the study volume, inability to retrieve three-dimensional structure, corruption of the mantle image by inadequate correction of the crust and boundary layer beneath, inability to retrieve true anomaly amplitudes, inhomogeneous ray coverage, and ignoring anisotropy (e.g., Anderson, 2011, Evans and Achauer, 1993, Foulger, et al., 2001, Keller et al., 2000, Masson and Trampert, 1997, Priestley and Tilmann, 2009, West et al., 2004). Some targets are simply not achievable using current techniques, particularly in remote oceanic regions. Perhaps the most vexed problem is assessing realistically the true errors in results. Because of the fundamental experimental setup, errors in structures calculated using teleseismic tomography are largest in the vertical direction. This results in a propensity to downward-smear structures, producing artificially vertically elongated anomalies. For surface-wave tomography, lateral resolution of anomalies is poorest so that lateral smearing is strong.

We have not dealt with the issue of anisotropy in this paper, and yet this effect may also be profound. The wave-speeds of both compressional and shear-waves (both SV and SH) are anisotropic in the mantle, and if this is neglected, which is usually the case, erroneous results and interpretations may result. Important targets for surface-wave tomography are determining upper mantle radial anisotropy, and azimuthal and vertical variations in wave-speed (Anderson, 1965, Gung, et al., 2003, Kustowski, et al., 2008, Lévêque, et al., 1998, Nakanishi and Anderson, 1984, Nataf et al., 1984, Tanimoto and Anderson, 1984). It is clear from surface wave studies that the upper 200 km of the mantle is the most heterogeneous and anisotropic region of the mantle, and that beneath this heterogeneity drops dramatically (Gung, et al., 2003). Many weak anomalies imaged by seismic tomography may result simply from uncorrected anisotropy. Anisotropy at ~ 200 km beneath cratons, and at ~80–200 km beneath ocean basins may be related to shear in the boundary layer, the difference in depth simply reflecting a variable depth to the maximum shear (Anderson, 2011).

In recent years, much progress has been made in improving computational techniques and incorporating these advances into tomographic practice. This includes using local structure in global parameterizations, and three-dimensional ray-tracing instead of assuming straight or piecewise-straight rays (Hung et al., 2001, Hung et al., 2004). Similarly, Christoffersson and Husebye (2011) have revisited the basics of the inversion methods used, showing that at least some of the often-noted smearing and weakening of velocity anomalies by traditional damped inverses can be mitigated by using better-tuned methods. Progress is also being made on describing better the uncertainties in the results, including calculating probability density functions (Mosegaard and Tarantola, 2002) (Sambridge, 1999, Sambridge, 1999). However, these advances cannot entirely overcome the fundamental difficulties we highlight above, which are inherent in the experimental setup. Improvements in inversion techniques can only make second-order improvements to the results. Nevertheless, there is a good case for re-processing many older data sets that have only been analyzed using older, more primitive methods, the results of which still influence dynamical models of the mantle.

In addition to computational challenges are the problems of presentation and interpretation of the results. The information in three-dimensional models is difficult to impart in a few maps and cross sections, and the wide array of choices such as which particular result to favor, and which

color palette, line of section, and zero-contour wave speed to select, means that there is broad scope for producing figures that support preferred models. The widespread use of relative wave speeds commonly leads to misinterpretations. Translation of seismic anomalies to geology is not straightforward. More physical parameters vary in the mantle than seismic parameters mapped, and simplifying assumptions, such as seismic wave speed being everywhere a direct proxy for temperature or density are not supported. Neither are geochemical models that rely on such work.

What is the way forward? First, the problem of imparting the results and calculable uncertainties is now solvable. Entire digital models, with errors, can be published on the internet, along with tools to enable authors to make their own plots and cross sections (Li, et al., 2008, http://www.earth.lsa.umich.edu/~jritsema/Research.html). Choice and responsibility is then transferred to the consumers of the results, and their challenge then becomes understanding the limitations of the results.

Second, notwithstanding the popularity of arrival-time tomography, there are many other seismic methods for studying the mantle that use wave amplitudes, whole waveforms, normal modes, combinations of data and either ray theory or full wave theory. In addition to wave speeds, attenuation and anisotropy can be derived. A fuller understanding of tomography results is achievable if all available data are used, along with robust tests of uniqueness to determine the space of plausible solutions.

Third, interpretive work should clarify which deductions are *required* by the data and which are not. Published, colored tomography images and simplistic, cartoon-like interpretations should be treated with skepticism. Blue colors in tomographic cross sections cannot be assumed to indicate cold, sinking material and red cannot be assumed to indicate hot, rising material. Likewise, increased awareness is needed that petrology/geochemistry cannot, in general, determine the depth of origin or temperature of magma sources. As a consequence, joint interpretation is more difficult than commonly realized. A more cautious approach will enable the current, unprecedented experimental tools available in both seismology and petrology/geochemistry to reliably contribute to answering fundamental questions about the structure and dynamics of

Earth's interior that have been disputed ever since plate tectonics was accepted and still remain controversial.

Acknowledgments

We thank Adam Dziewonski, Rob van der Hilst, Jeroen Ritsema and Don Anderson for helpful comments on a draft manuscript. GFP thanks Progetto Quadro Regione Friuli Venezia Giulia "Definition of seismic and tsunami hazard scenarios by means of Indo-European e-infrastructures", and the Italian PNRA and PRIN for partial financial support of the research that led to some of the results discussed in this paper. IMA acknowledges research grant FNU-31402. ML acknowledges grants AST 2008, 2009, Ateneo 2010, 2011, and MIUR-PRIN 2008 (Grant no. 2008HMHYFP_005).

Appendix 1: Tomography Perils and Pitfalls

Many issues arise when interpreting a tomographic model. It is a highly imperfect “lens” with which to view Earth. The extent and causes of this imperfection are understandably vague for geologists, geochemists, and others outside the specialty, but even many currently active tomographers seem to be unaware of many of its perils and pitfalls or to misjudge their extent.

Here we restrict ourselves to a terse description of issues arising in teleseismic tomography, the use of the terminal portions of *P*, *S*, and core phases to estimate regional wave speed structure (or *Q*) beneath a seismograph array. It is the earliest, simplest, and most linear of current tomography methods. In this Appendix we do not address local-earthquake or global tomography, which are highly nonlinear problems due to the presence of ray turning points inside the model volume. The presence of turning points leads to first-order interactions between wave speed and raypaths, requiring a conservative approach to the inversion process and serious risk of falling into a "local minimum", i.e., a solution that is far from broadly optimal. Neither do we address surface-wave tomography or methods used in refraction or reflection seismology, though analogous problems will be present, generally turned 90° from those discussed here.

Background: What is tomography?

The data used are variations from some norm in the arrival times of *P, S*, or some other phase from distant earthquakes, as received at an array of seismographs that overlies the "target volume". For teleseismic tomography, the target volume comprises some portion of the crust and upper mantle for which one wishes to know the wave-speed variations. In practice one uses relative travel-time variations (typically relative to a mean delay or advance relative to some whole-Earth wave-speed model for that given earthquake and phase, the "norm"). This reduction is permissible because teleseismic tomography cannot recover absolute velocities in the target volume, and it is desirable because it improves the accuracy of the measured traveltime variations.

One next creates some description of an initial wave-speed structure inside the target volume. That structure inevitably simplifies the volume and its structure, commonly into a set of constant-wave-speed blocks or nodes, each given initial wave speeds that are reasonable for that

part of the world at that depth (to put the rays in the right places). Those initial wave speeds typically are for a simple layered Earth model. This rather profound simplification of Earth wave-speed structure into blocks It or nodes within a layered Earth is called "parameterization" and imposes substantial restrictions and assumptions on the structure one eventually computes, imperfections that are not explicit in the subsequent mathematical solution.

The computation itself is a fitting process, equivalent to fitting a line to a scatter plot. (Indeed, deciding *a priori* that the scattered data must express some simple line is the equivalent of parameterizing the tomographic model and, of course, can be anywhere from a good approximation to nonsensical. Regardless, any functional form is bound to be simpler than reality in a system as complex as the Earth.) The tomographic fitting process then extracts the best fitting wave-speed variations for each block or node in the parameterized target volume, based upon the traveltime data and where the associated rays travel within that volume.

Up to now, the mathematical fitting methods used, "the inversion", typically use a least-squares fit with additional constraints beyond the observed data (typically by "damping" either the amplitude or smoothness of the model). Those additional constraints are required to select a particular result from an infinite number of possible ones (infinite for various mathematical and physical reasons, as showed for example by Backus and Gilbert (1970, 1967, 1968). The selection of an additional constraint also can cause and obscure uncertainties in the resulting wave-speed model. So in addition to formal measures of fitting accuracy yielded by the inversion procedure or tests with synthetic data sets, one has to account for the effects of parameterization, selecting the additional constraint, and the inability of telesiesmic tomography to extract absolute velocity. However, none of these appear in the numerical result in any clear manner if at all.

Resolution Perils and Pitfalls–General

The resolution capabilities of a given data set (set of timed rays at various locations, backazimuths, and inclinations) must be tested, evaluated, and understood in detail. However, at present such matters typically are only tested in a cursory, optimistic manner. It is never sufficient to evaluate only the diagonal elements of **R** (the resolution matrix) or equivalent techniques for inversion methods not generating an explicit **R**. Many of these issues are tested numerically and illustrated in the following section.

A widely used technique for estimating the resolving capabilities of a teleseismic tomography data set is to create a synthetic data set of travel time residuals for a checkerboard wave speed structure (horizontally alternating blocks of high and low wave speed). However, all damped teleseismic models have resolution kernels (equivalent to a column of **R** or the result for a synthetic model containing a single anomalous block) that oscillate along the horizontal direction. That is, they have negative values adjacent to the block of interest as well as smearing positively above and below the block (Figure A1). Because of the shape of such resolution kernels, teleseismic tomography is highly compatible with horizontal-checkerboard structures. Put bluntly, checkerboard tests are the most optimistic possible evaluation of resolution. Actual resolution is inevitably worse, often much worse, for real Earth structures. Some of the inherent drawbacks of the use of checkerboard tests may be overcome by checking the degree to which synthetic models of the main features in the interpreted model may be recovered from inversion of synthetic travel-times (e.g., Alinaghi, et al., 2007). This approach allows the interpreter to test if specific features of the velocity model may be fully or partly recovered by the same ray geometry as in the real data.

At a minimum, proper evaluation of **R** requires one to understand the single-block "impulse" response (resolution kernels) resulting from the data set and to do this separately for all major regions of the model (Figure A2). Resolution behavior generally can be assumed to be roughly similar within each of these regions and to vary more or less smoothly between them. Note especially that **R** and its kernels always will be poor below a depth approximately equal to the array aperture, and will also be poor in the periphery of the model, beyond the array bounds. In these areas ray crossfire inherently is limited, and nothing can improve the situation. With a good data set, in such location one may be able to infer that some wave speed structure lies along the dominant ray bundle at some distance anywhere from the surface to well beyond the model boundary, but there is no way to determine where the anomaly is along the ray bundle. Furthermore, systematic timing errors, real anomalies outside well-resolved areas, and even strong anomalies within the well-resolved area commonly smear into these poorly resolved regions to satisfy the inversion's damping term by roughly accounting for those features of the travel times with weak, distributed features far from the true causal anomaly. Features in these areas are, therefore, always artifacts or indistinguishable from artifacts.

There are also widespread misconceptions of what constitutes a "good" set of observed rays (or of first-Fresnel zones, not distinguished here because they simply affect a smoothing operation so mainly benefit second-order features near the model's noise level). An optimal teleseismic tomography data set must everywhere contain roughly equal numbers of rays in all ray orientations and locations. That is, the number of rays is less important than their distribution of orientations at any given location in the model.

A common, related trap results from inhomogeneous source-event distribution, that is, from using data sets with most rays in bundles that have only a subset of possible orientations. For example, in the western U.S., nearly all viable rays originate along the Pacific rim (northwest, southwest, and southeast *P* and *S*) or at distances above ~140° (near-vertical core phases). In contrast, the northeast azimuth has very few earthquakes and inevitably has very few observed rays of good quality and fewer per event even when observable. Additionally, rays from the SW mostly come from deep sources in the south Pacific yielding impulsive waveforms that can be timed more accurately than the shallow-source phases available from the NE. This situation is equivalent to a properly "reversed" NW-to-SE-directed refraction line but an "unreversed" SW-to-NE-directed line. Features on the SW-NE plane always will be poorly resolved and strongly smeared along *P* and *S* ray bundles from the SW as well as, sometimes, vertically along the core phase bundle. Subsetting the SW ray set leaves that bundle observed with lower-noise data than NE body waves, which are lower in timing accuracy. This quality asymmetry leads to lesser but similar bias to the imbalance in ray count.

The effects of misconceptions and inadequate analysis of **R** turn up regularly in the literature. In particular, recent inferences of deep (deeper than the array aperture) low-wave speed anomalies beneath Yellowstone and Hawaii are likely either artifacts or indistinguishable from artifacts. Claiming these features as evidence of plumes from the core-mantle boundary, or other deep sources for "hot spots", is unsupported by the data. The only viable evidence we have seen for melt or compositional variations beneath "hot spots" is above the upper-mantle discontinuities. Furthermore, there are several interpretations that imply dipping structures in regions where rays are dominated by one bundle of *P* or *S*–such "dipping" also is an artifact or indistinguishable from an artifact.

Resolution Perils and Pitfalls–Numerical Examples

All tomographic solutions are inherently smoothed. It is impossible to obtain a precise local solution everywhere because not all points of the medium are crossed by raypaths or are not crossed by rays that are widely distributed in orientation. In both cases, information about wave speed in such areas is weak, absent, or spatially distorted. The degrees of smoothing and distortion at a given location determine useful resolution and the limits of meaningful interpretation.

Even in the limit where the resolution matrix **R** is the identity (**R** = **I**; all parameters perfectly resolved), wave speed anomalies within blocks (or surrounding and contributing to nodes) are at least smoothed within those block volumes, and the degree of that smoothing is determined by block size (or node spacing) which is determined by ray coverage. In reality it is impossible to achieve such “perfect” resolution (Backus and Gilbert, 1970, Backus and Gilbert, 1967, Backus and Gilbert, 1968) and difficult even to approach that ideal. Thus, an estimate of the best possible resolving power at any location is the volume and shape of the averaged region at each location; those "impulse response" volumes will vary across the model depending on local ray density and how evenly those rays are distributed in position and orientation.

In Figure A3(d),(g), a simple synthetic model where the ray-orientation distribution is almost uniform and from all sides, the averaging area can be approximated by a circle or sphere–the “volume-of-averaging area”. When the rays have an uneven distribution of orientations (the usual case around the edges of any teleseismic tomography model and below a depth about equal to the aperture of the observing array), then the volumes resolved will be stretched along the predominant ray direction. The simplest approximation of the “resolved” volume in this case is an ovoid (or in two-dimensions an ellipse). Resolution will be least along the major axis of the ovoid and best along the minor axis. The aspect ratio of such ovoids can be quite large.

This variation in the “resolvable ovoid” and corresponding diag(**R**) are illustrated by two-dimensional synthetic examples in Figure A3(*a*)–(*n*). Sources and receivers are present on all sides of that model area; in teleseismic tomography the stations are at the surface and sources effectively along the bottom of the model, making the situation worse. Starting models of wave speed are shown in (*c*), (*f*), (*i*), and (*l*) for various arrangements of low- and high-wave speed

anomalies, including checkerboard and anti-checkerboard models. Travel times were calculated for the two sets of raypaths in (*a*) and (*b*), respectively good and poor ray distributions. Both ray distributions are poor at the periphery. No random noise was added to the synthetic travel times. Had it been added, useful resolution would be worse.

In Figure A3(*a*) and (*b*), green areas are the resolvable ellipses (Yanovskaya, 1997) centered on several of the true anomalies. For the good set of raypaths (*a*), these averaging areas in the central area are approximately circular and centered at the original anomalies (the azimuthal distribution of paths is most uniform here). However, near the periphery, especially in the corners, the ovals are elongated parallel to dominant ray directions (effectively radial). Thus, the tomographic reconstruction of wave speed anomalies near the centers of (*d*), (*g*), (*j*), and (*m*) are faithful, but for the poor ray set used in (*e*), (*h*), (*k*), and (*n*), yield badly distorted features even near the center. All are stretched in the direction of the most numerous rays. In particular, the ray set in (*b*) has semi-parallel rays along the "southwest-northeast" diagonal, and the resolvable ellipses are elongated along the diagonal and large. Thus, the wave speed anomalies in (*e*), (*h*), (*k*), and (*n*) are both badly smeared along the diagonal and weakened relative to the good ray set.

A number of the original anomalies effectively vanish or have lowered estimated wave speed perturbations. Even with the good ray set, estimated perturbations between anomalies of the same sign (anti-checkerboards of (*f*) and (*l*)) bias toward the adjacent values, with individual features effectively vanishing in (*h*) and (*n*) and merging with like-sign neighbors and weakening in (*e*), (*k*), and (*m*) and even in the corners of (*j*). Wave speed estimates midway between anomalies fall to zero (rather to the layer mean wave speed) where those anomalies are of opposite sign, as in (*d*) and the north–south direction of (*g*). The midpoints between like-sign anomalies are biased to the same sign, as in (*g*), (*j*), and especially (*m*).

The dense-anomaly results in (*j*) and (*m*) illustrate checkerboard optimism. The wave speed sign alterations in (*j*) are more-or-less recovered at the center of the model but those in (*m*) are recovered only in the north–south direction and merge into single anomalies east–west. The well-observed, effectively isolated features in (*d*) and (*g*) are recovered fairly well regardless of sign. Even so, points midway between like-sign anomalies bias toward the sign of the neighboring

anomaly. These isolated features simulate impulse responses for each feature with only the low-amplitude edges of kernels merging.

The distributions of true anomalies in Earth thus have a first-order effect on the ability of the data set to resolve those anomalies. Checkerboard tests do not illuminate such effects. On the contrary, they tend to mask them. An example of the problems for a real experiment is illustrated in Figure A4. This shows the results of inverting a synthetic dataset similar to that collected in the Ethiopian rift by Bastow et al. (2008), to test the ability of the experiment to retrieve a structure comprising a pair of high-wave-speed rift flanks. A strong zone of low wave-speed is imaged between the flanks, that did not exist in the original structure. This entirely fictitious body would be readily interpretable in terms of geology.

Cryptic Perils and Pitfalls

In addition to the well (if not widely) understood problems with **R** described above, we note the following:

(1) **R** truly is singular. It is a "lens" that cannot be corrected for or "seen through" any better than is described formally by **R**, and often far less well than common tests of **R** suggest.

(2) Long sums of small numbers (small off-diagonal values in any kernel of **R**) can cause artifacts that many do not recognize or consider. In the extreme, these off-diagonal elements sum to large positive values that effectively smear all evidence of absolute wave speeds across the entire depth range of the model, rendering them invisible. The same phenomenon is present when modeling broad lateral variations in wave speed, such as a horizontal low-wave speed "lens" embedded in an otherwise featureless background (as may be present near the Moho beneath the Yellowstone caldera and certainly is present as low-speed breccia, tuff, hydrothermally altered rock, and other materials filling surface calderas). The edges of the horizontal lens will be located correctly and characterized by a doublet anomaly in the horizontal direction, where the peak-to-peak speed range of the doublet is approximately equal to the (damped) perturbation within the lens. However, absolute wave speeds vanish, such that positive and negative peaks of the doublet have similar magnitudes. This is so, again, because damped inversions have negative side lobes in the kernels of **R** in horizontally adjacent blocks. Furthermore, the center of the lens is eviscerated and spread into a tall, very

weak diamond-in-X pattern of apparent perturbation, as discussed by Evans and Achauer (1993, their Figure 13.7, upper right panel).

(3) Because it is impossible to recover absolute wave speeds with teleseismic tomography, all "high" and "low" wave speeds calculated are relative to some unknown, unknowable wave speed. For example, it is incorrect to characterize areas surrounding a thermo-compositional low-wave speed anomaly as "fast". These peripheral areas may, in fact, be near or even below typical Earth model wave speeds despite their apparent elevation (see also Section 3.1).

(4) More insidious still are the cryptic effects of parameterizing the wave speed model and the various other approximations and assumptions required to make the inversion realizable and unique. These effects have been known since the beginning of tomography, illustrated for example, by the inversion for a single-block anomaly. The structure is rendered well when it matches the location of a model block, but vanishes when it straddles adjacent model blocks (Ellsworth, 1977). There simply is no escaping the fact that Earth does not comprise layers of blocks or nodes, nor is it damped, nor can the resulting model be uniquely selected from the infinite set of possible solutions. While some authors appear to believe that **R** is truth, full and precise, it is not, and the differences can be substantial, invisible, and insidious.

(5) Cross-correlation phase-picking methods have come into nearly universal use, commonly using the method of VanDecar and Crosson (1990). However, these methods inherently disregard physics and known Earth structure. In particular, the first 10 to 20 s of *P*, and a similar range before and after the first arrival of *S*, are contaminated by systematic signals from crustal and upper mantle converted phases and multiples. If they were not so contaminated, receiver function analysis would be impossible. Furthermore, diffracted phases passing around strong anomalies are present before or after the direct ray and may mislead the analyst or subsume additional systematic errors into cross-correlation picks (inversions generally assume that the direct phase is measured). While such errors are unavoidable, they are smallest during the largest early half cycle of the direct phase (generally the first or second large half cycle). Diffracted and converted phases are commonly an order of magnitude smaller during this peak-signal interval, yet when summed over a wider correlation window become significant (again, the sum of many small numbers). Worse yet,

because these errors are systematic (deterministic) they must map into the inversion result somewhere. Unfortunately, where they will map is essentially unknowable, although they may affect poorly-resolved regions more because in well-sampled areas redundant sampling of anomalies will suppress expression of these errors. Thus, no travel-time picking method should be used that does not, at least in its final step, correlate only the first or second strong half cycle of the direct wave (as is easily done in the method of Lou et al., 2013).

Lou et al. (2013) describe a revised correlation picking method and associated software that makes central the use of a stacking the target-phase records, thus improving the analyst's ability to judge the quality of the data. In addition to relative traveltimes, their method (1) returns robust absolute first-arrival estimates, which may be used to constrain the mean structure of the region, and (2) makes it feasible for the analyst to restrict the correlation window to the first large peak or trough of the phase in question (e.g., their Figures 2a and 3b). We consider this essential for accurate data analysis and all that follows. Because correlation squares the signal, the high amplitudes of the direct-phase first arrival and relative absence of the lower amplitudes of contaminating phases within this narrow window makes these picks as accurate as can currently be done. Though largely automatic, the method of Lou et al. (2013) requires the analyst to look at every event and apply their judgment rather than blindly trusting of an algorithm to determine picks and their qualities. In our experience, far too many things happen in deployed instruments and the Earth for an algorithm to be reliably used as a black box. The software provided by Lou et al. (2013) makes implementation of their method straightforward, and we recommend its use.

(6) One corollary to (5) is that a human being must verify all arrival-time measurements by inspection, removing or correcting those that fall prey to “cycle skipping”, seismograph problems such as polarity reversals, crossing phases, local noise bursts, and so forth. An independent test of data quality can be made by plotting the observed relative residuals at each station onto a lower-hemisphere plot according to the ray approach direction beneath the station. In such a plot, strong, isolated travel time anomalies are candidates requiring additional manual review to confirm or remove them from the data set. Obviously, the seismograms take precedence to such “polar plots”, or one risks “cooking” the data.

(7) Damping may be too low (resulting in the same checkerboard or patchy pattern discussed above) or too high (resulting in underestimated anomaly amplitudes). Furthermore, there is now good evidence that damped inversions always significantly depress the amplitude of recovered anomalies even when damping is chosen optimally (see also Section 2.5) (Christoffersson and Husebye, 2011). The significance of this effect can be assessed using model-driven resolution tests.

(8) Scaling of the wave speed scale, particularly when the most anomalous regions saturate, is suspect. Authors must at the least present a range of scaling options in e-supplements to any tomography paper, and should in the body of the paper show at least some unsaturated plots to demonstrate the relative strengths of various claimed features (see also Section 4).

Implications

The effects of these perils and pitfalls upon discussions, in particular of “hot-spot” origins, has caused widespread confusion and resulted in interpretations not supported by the data. What is clear from teleseismic tomography and other methods is that most “hot spots” are underlain by relative low-wave speed anomalies that may appear to largely or fully terminate at ~200-600 km depth, commonly near an upper-mantle discontinuity or the bottom of the LVZ.

It is not clear, however, whether various proposed features below this ~200-600 km upper-mantle depth are meaningful or are simply artifacts of the method, the particular ray sets used, and the strength of shallower anomalies. Indeed, well-established highly anomalous crustal and upper-mantle structures are certain to smear outward into these poorly resolved parts of models and to be partly or entirely responsible for deeper apparent anomalies. Many similar features were noted and disregarded by the most experienced tomographers decades ago, simply because these deeper features were recognized as uninterpretable, either artifacts or indistinguishable from artifacts.

We consider all proposed deeper anomalies at "hot spots" to date to be unconvincing, and see no good evidence of wave-speed anomalies below a few hundred kilometers depth. Our shallow-only conclusion is most easily explained either as a near-solidus bottom-up source in the upper mantle, or as a surface-down penetration to no deeper than about the upper-mantle

discontinuities. Given similarly strong reservations about global-tomography models, in part because of their inconsistent results and very weak perturbations, leaves only one known test for deep, weak, low-wave speed conduits in the lower mantle beneath “hot spots”–by using a very wide aperture experiment, or by looking for guided waves traveling within the conduit (Julian and Evans, 2010). Several suitable datasets exist for this method, for Yellowstone, Iceland, and Hawaii.

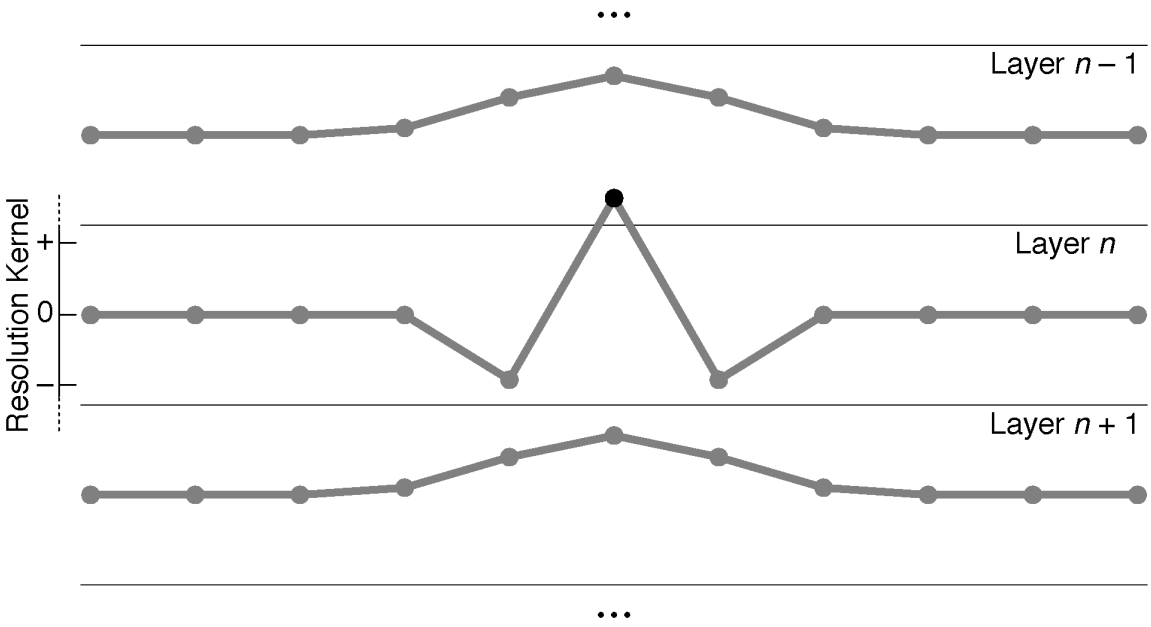

Figure A1: Schematic of a portion of one typical kernel (column) of **R** for a block or node at the center of layer *n* for a typical teleseismic tomography study (gray lines and dots) showing the relative magnitudes of diagonal (black dot) and off-diagonal (gray dots) elements of **R**. These dots are (horizontally) at block centers and vertically proportional to the amplitude of **R** in that element (relative scale at left). Such representations can be thought of as the "impulse response" to the presence of a single-block anomaly at the center of layer *n*, for the filter comprised of a particular dataset and (to a lesser degree) the particular inversion method used.

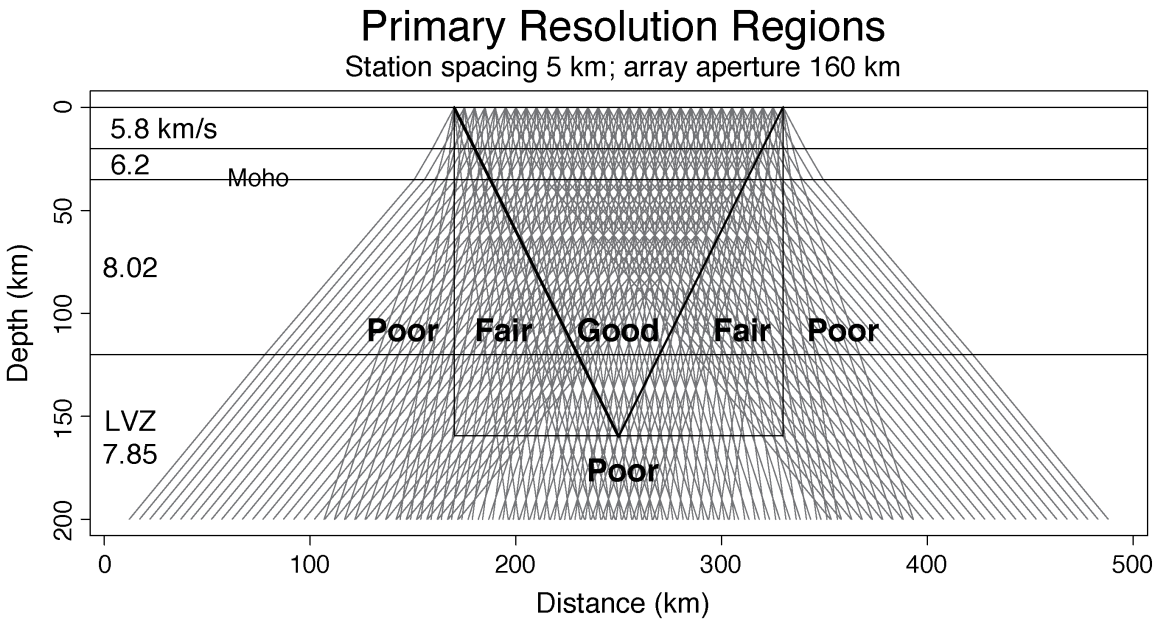

Figure A2: Typical but idealized two-dimensional ray set for teleseismic tomography. Arbitrary scaling; no vertical exaggeration (after Evans and Achauer, 1993).

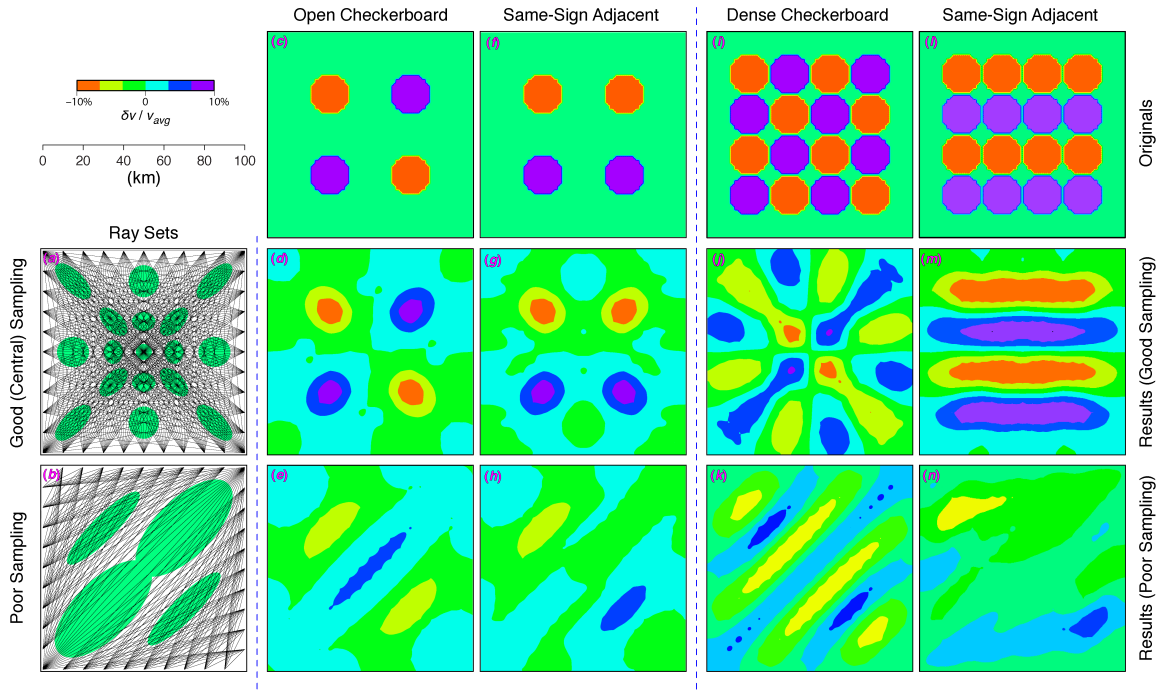

Figure A3: Two-dimensional synthetic-data tests of resolution for (*a*) a best-case and (*b*) more typical ray sets, with similar numbers of rays in each. The models used to create synthetic travel times are in (*c*), (*f*), (*i*), and (*l*). Inversion results using the best-case ray set are in (*d*), (*g*), (*j*), and (*m*) and those for the more typical ray set are in (*e*), (*h*), (*k*), and (*n*). Green ovals in (*a*) and (*b*) are estimated minimum-resolvable objects in various locations (from Yanovskaya, 1997).

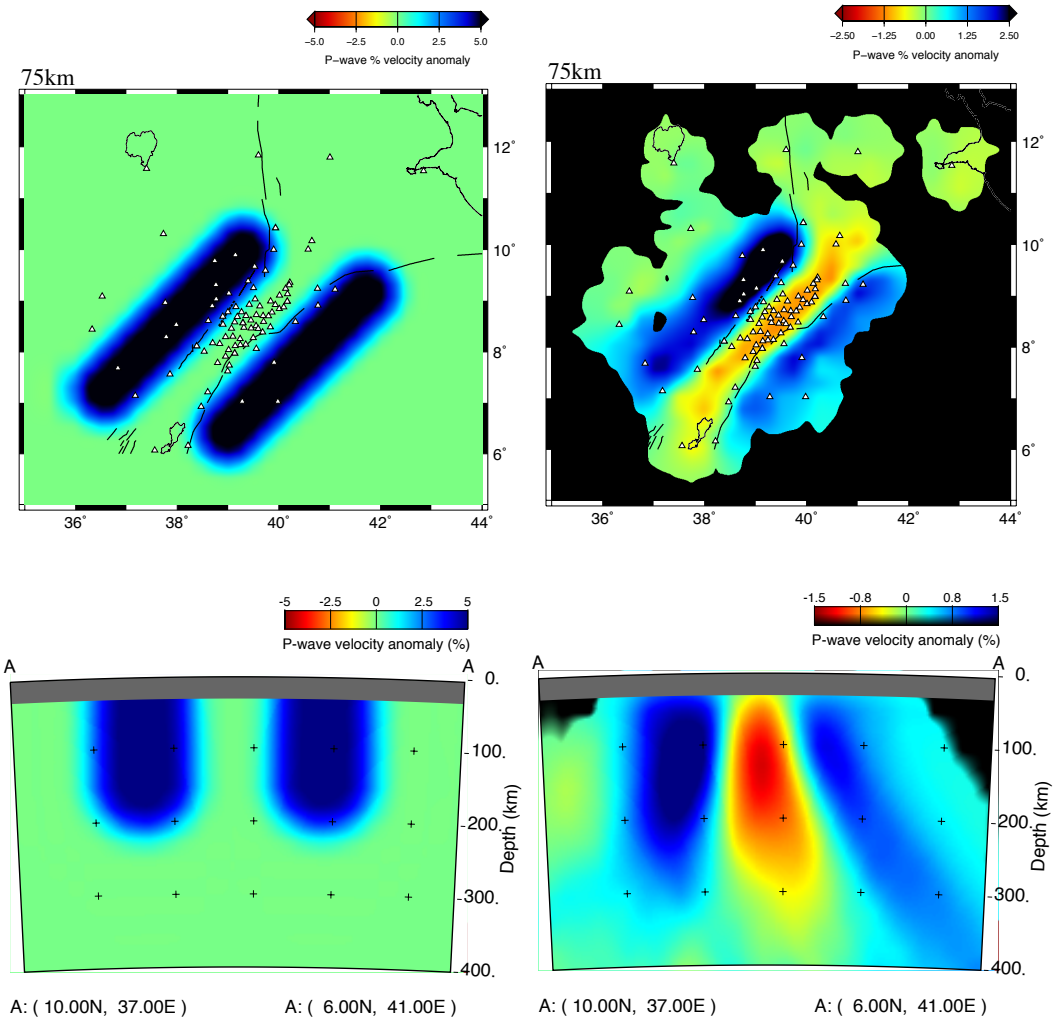

Figure A4: Synthetic wave-speed model for the Ethiopian rift (left) consisting of high-wave-speed (Δv_P =5%) rift flanks. A relative-arrival-time dataset is computed for the same station-earthquake pairs used in the study of Bastow et al. (2008). The resulting tomographic model is characterized not only by fast wave-speed flanks but also by a low-wave-speed zone beneath the

rift valley. In reality, in Ethiopia, *P*- and *S*-wave arrival times are ubiquitously late compared to the global mean, with the implication that the "high" wave-speed (blue) regions are low wave-speed compared to the global mean (Bastow, 2012, Bastow, et al., 2008). A model result with high- and low wave-speed structure is the inevitable consequence of relative arrival-time inversions.

Table 1: Typical reductions in v_P and v_S for plausible variations in composition, degree of partial melt and temperature in the mantle. T_m: solidus temperature.

Phase	Partial melt (per 1% increase in melt content)*	Composition (per 4% reduction in Mg#=Mg/(Mg+Fe) in olivine)§**	Temperature (per 100 K increase)*** $T < 0.8\ T_m$	Temperature (per 100 K increase)* $0.8\ T_m < T < 1.1\ T_m$
v_P	1-3%	7%	1%	up to 10%
v_S	3-10%	12%	1.5%	up to 10%

* Depends critically on melt geometry. Numbers in the table refer to laboratory experiments. A significant shear wave velocity decrease, such as observed in the LVZ, can be produced by very small, unconnected grain boundary melt fractions (Faul and Jackson, 2007, Mavko, 1980, Murase and Fukuyama, 1980, Murase and Kushiro, 1979, Murase et al., 1977, Schmeling, 1985).
** Numbers in the table account for compositional variations in iron-content only. Other compositional and mineralogical effects may also be influential. For example, in cratonic roots, iron-depletion is often correlated with orthopyroxene-depletion, which may have the opposite

effects on seismic velocities. This may cancel out, or even reverse the effect of iron depletion (Artemieva, 2011, Jordan, 1979, Lee, 2003).

*** (Kern, 1978, Sumino and Anderson, 1982).

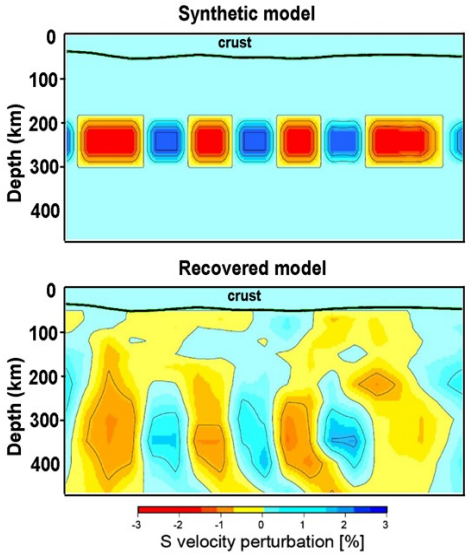

Figure 1: Depth leakage (downward smearing) in a seismic tomography inversion (after Eken, et al., 2008).

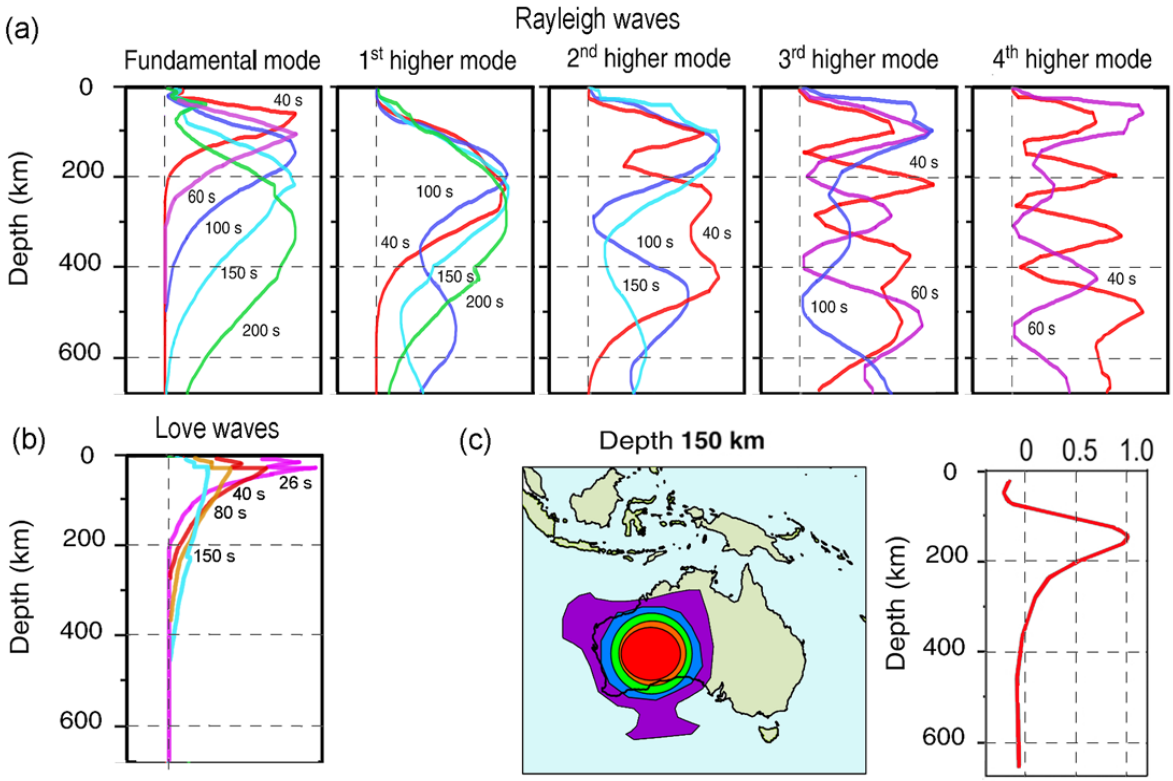

Figure 2: (a) Sensitivity kernels (normalized to a maximum amplitude of 1) which relate Rayleigh-wave phase wave speed of the fundamental mode and the overtones to shear wave speed for the PREM model (after Ritsema, et al., 2004). (b) Love wave sensitivity at different periods with respect to horizontal shear wave speed variations (after Curtis et al., 1998). (c) Backus–Gilbert resolution kernels for global surface-wave tomography model S20RTS for a point beneath Australia at 150 km depth (left, lateral resolution) and the radial dependence of the resolution kernel (right, vertical averaging in the final model. After Ritsema, et al., 2004).

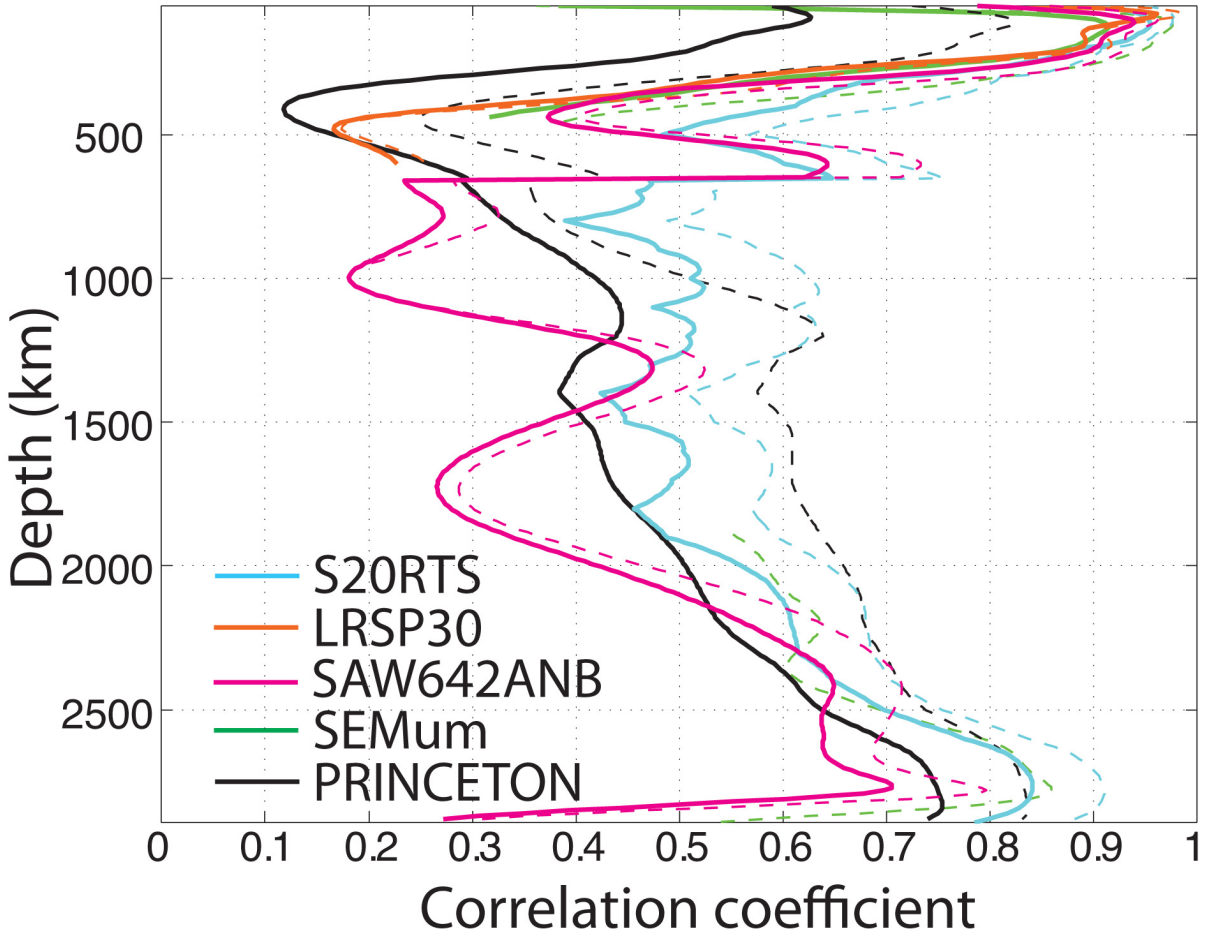

Figure 3: Correlation coefficients between several v_S models (Cammarano, et al., 2011).

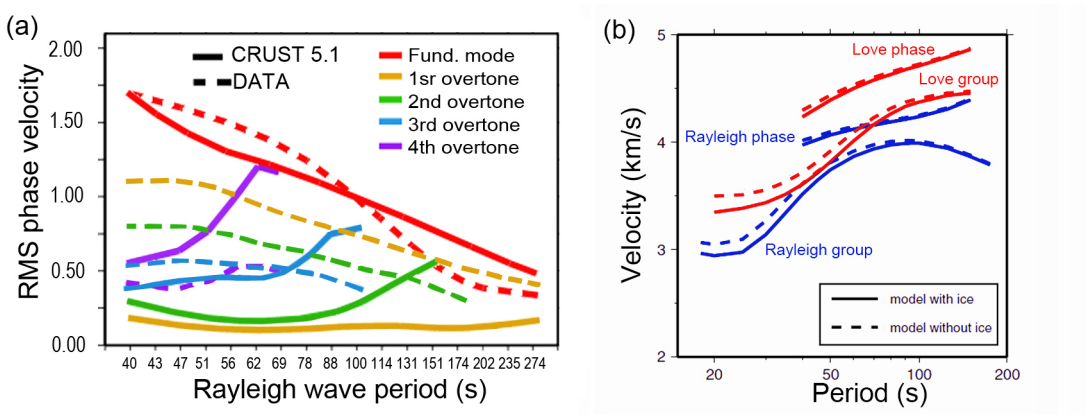

Figure 4: (a) Root-mean-square phase wave speed perturbation of the Rayleigh wave with respect to PREM (in %) in the data (dashed lines) and produced by crustal correction (solid lines) for the CRUST 5.1 model (Mooney, et al., 1998, Ritsema, et al., 2004), (b) the effect of the ice sheet on surface wave velocities (after Ritzwoller, et al., 2001).

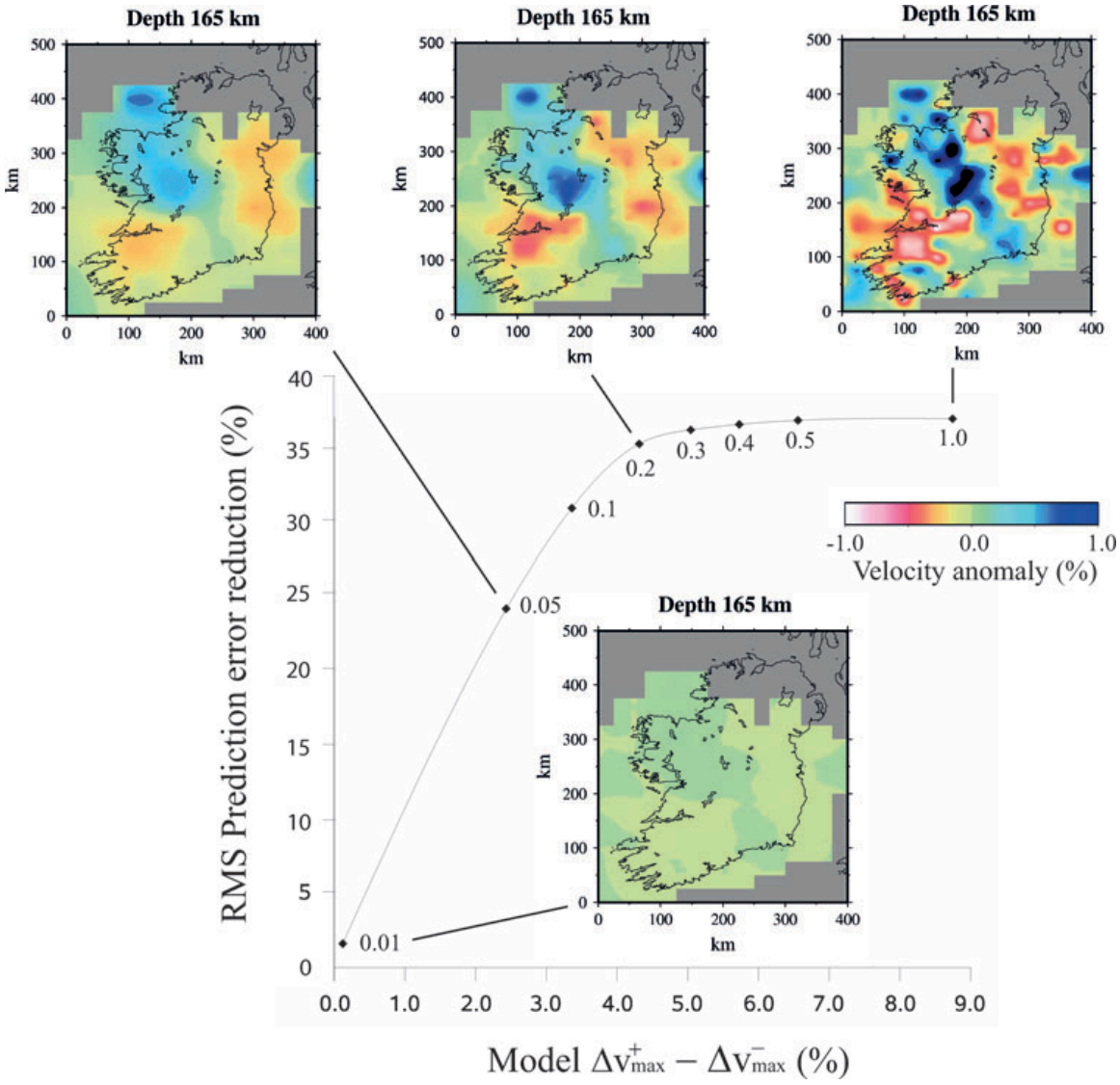

Figure 5: Trade-off curve showing the balance between model roughness (quantified by the difference between the extremal positive and negative wave speed contrasts, $\Delta v^{+}_{max} - \Delta v^{-}_{max}$) and root mean square prediction error reduction (%). The curve is labeled with wave speed model parameter standard deviations. Each point represents a model solution corresponding to the indicated model parameter standard deviations (from O'Donnell, et al., 2011).

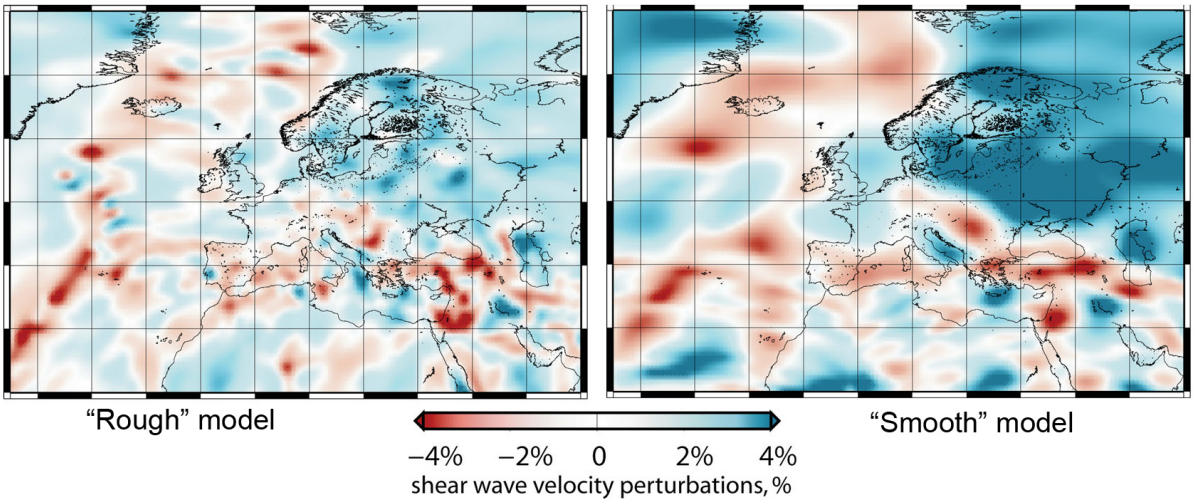

Figure 6: The effect of smoothing on mantle velocity structure. The example refers to 110 km depth; the model is constrained by non-linear waveform inversion (Legendre, et al., 2012).

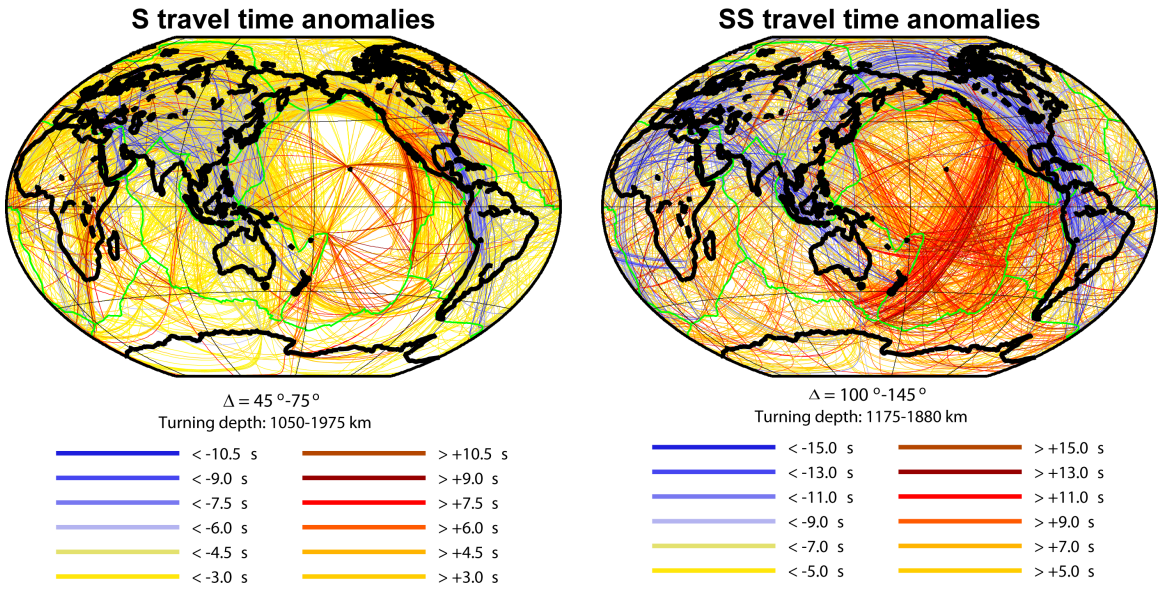

Figure 7: *S* and *SS* raypaths sampling the mid-mantle. Much of Earth's interior is effectively unsampled, and much else is sampled primarily by sub-parallel rays rather than by the diversely crossing rays required for good tomographic imaging. The so-called deeply subducted “Farallon slab” (Grand et al., 1997) beneath the Caribbean and eastern United States is particularly non-uniformly sampled. Published tomographic images of this region vary greatly (). (Figure provided by Jeroen Ritsema and published in Hamilton, 2011).

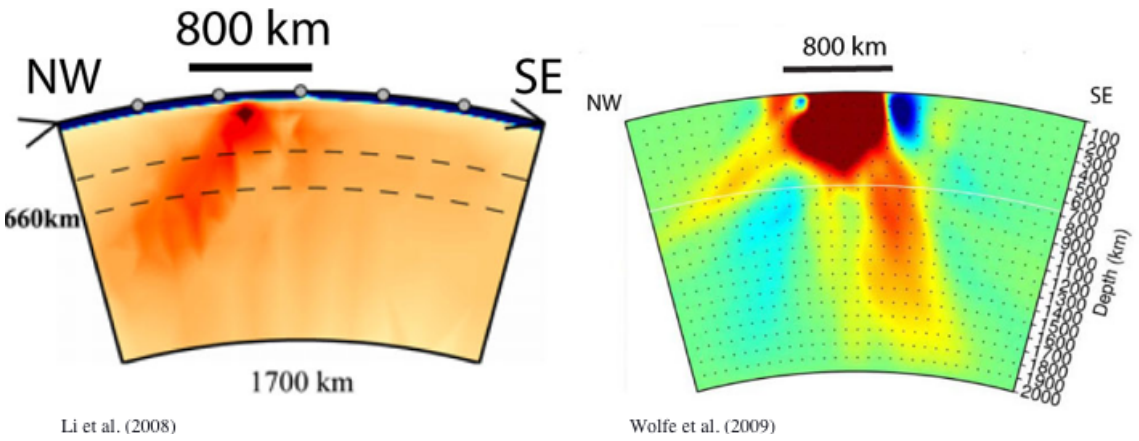

Figure 8: An example of the absence of repeatability. Two tomography "images", each show a downward-elongated low-wave-speed region beneath Hawaii. One plunges to the north-west and the other to the south-east. Both were interpreted as a mantle plume (left; Li, et al., 2008; right, Wolfe, et al., 2009). The study illustrated at left used ak135 (Kennett, et al., 1995) as a starting model, and the study at right used IASPEI91 (Kennett and Engdahl, 1991) as a starting model.

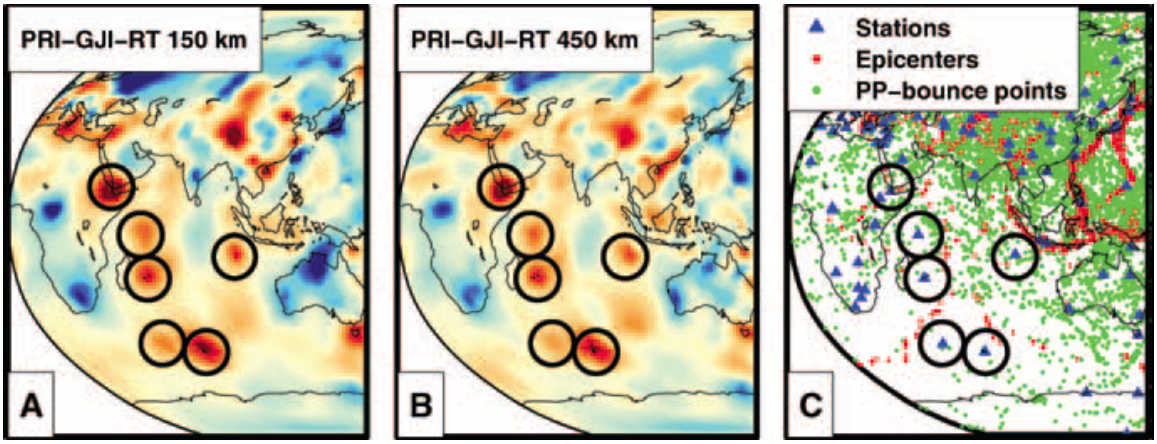

Figure 9: Map of *P*-wave speed at 150 km (left) and 450 km depth (middle) beneath the Indian Ocean according to model PRI-GJI-FFT (Montelli, et al., 2006, Montelli, et al., 2004, Montelli, et al., 2004). They are almost identical, suggesting they arise from quasi-parallel bundles of up-coming rays. The geographical distribution of sources (red dots), receivers (blue triangles), and *PP* bounce points (green dots) depicted in the right panel show that ray sampling is sparse in much of the Indian Ocean except immediately beneath seismic stations deployed on islands (from van der Hilst and de Hoop, 2005; see also http://www.mantleplumes.org/BananaDoughnuts.html).

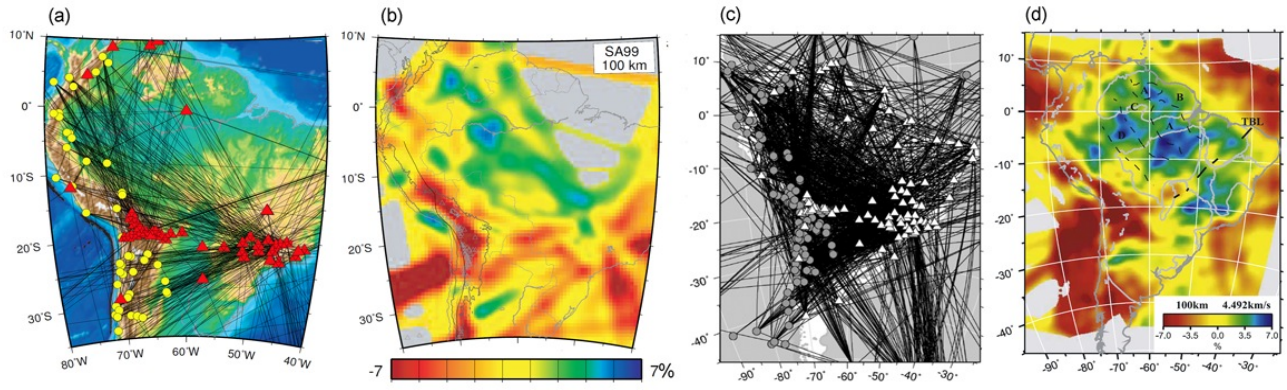

Figure 10: Wave-speed perturbations with respect to IASP91 (Kennett and Engdahl, 1991) at 100 km depth beneath South America (b, d) and the corresponding raypaths for Rayleigh waveform data (a, c) (c-d from Feng, et al., 2007, a-b from van der Lee, et al., 2001).

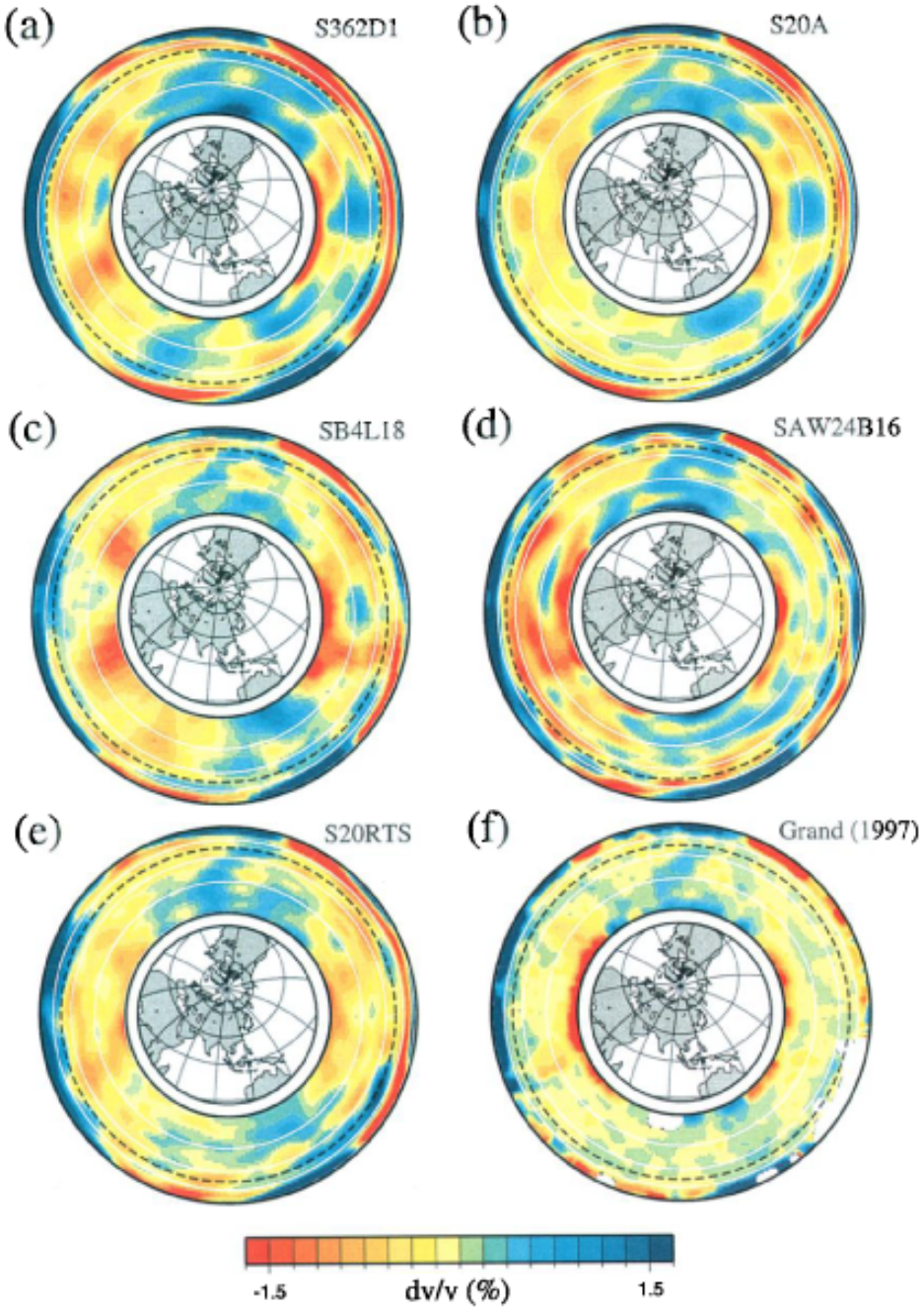

Figure 11: Cross sections from six whole-mantle tomography models. The complex wave speed pattern under North America and the eastern Pacific cannot be fully accounted for by simple subduction of the Farallon slab. However, it is clear that support for different models of mantle

structure and dynamics can be claimed, simply by choosing a preferred result (from Gu, et al., 2001).

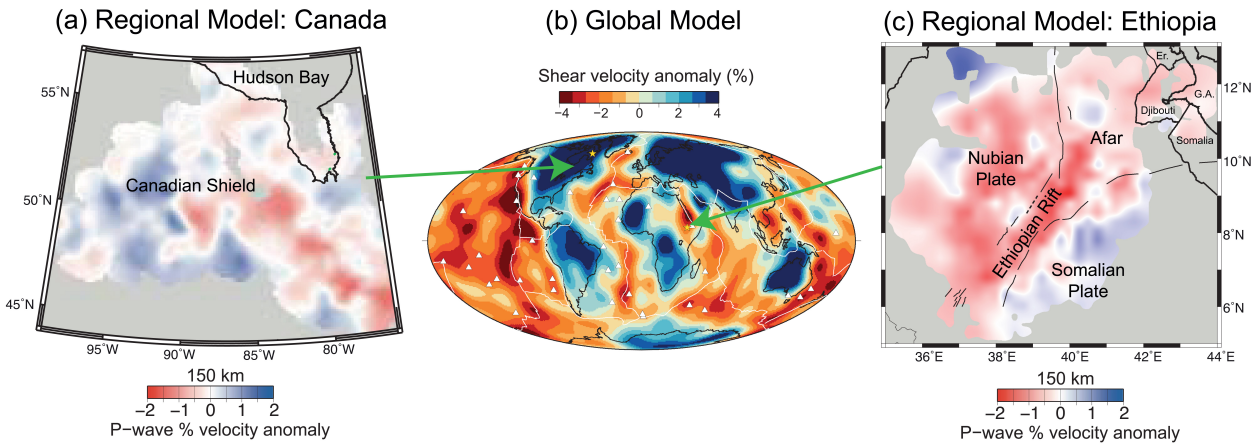

Figure 12: A comparison of global and regional tomographic models. Panel (A) Slice at 150-km-depth through the P-wave relative arrival-time tomographic model of Frederiksen et al. (2007) in Canada, computed from the inversion of relative arrival-time residuals. Panel (B) Slice at 150-km-depth through the global tomographic model of Ritsema et al. (2011).White lines are plate boundaries. Panel (C) Slice at 150-km-depth through the P-wave relative arrival-time tomographic model of Bastow et al. (2008) in Ethiopia, computed from the inversion of relative arrival-time residuals. Dark lines are mid-Miocene border faults that define the Ethiopian Rift. Areas of poor ray coverage are black.

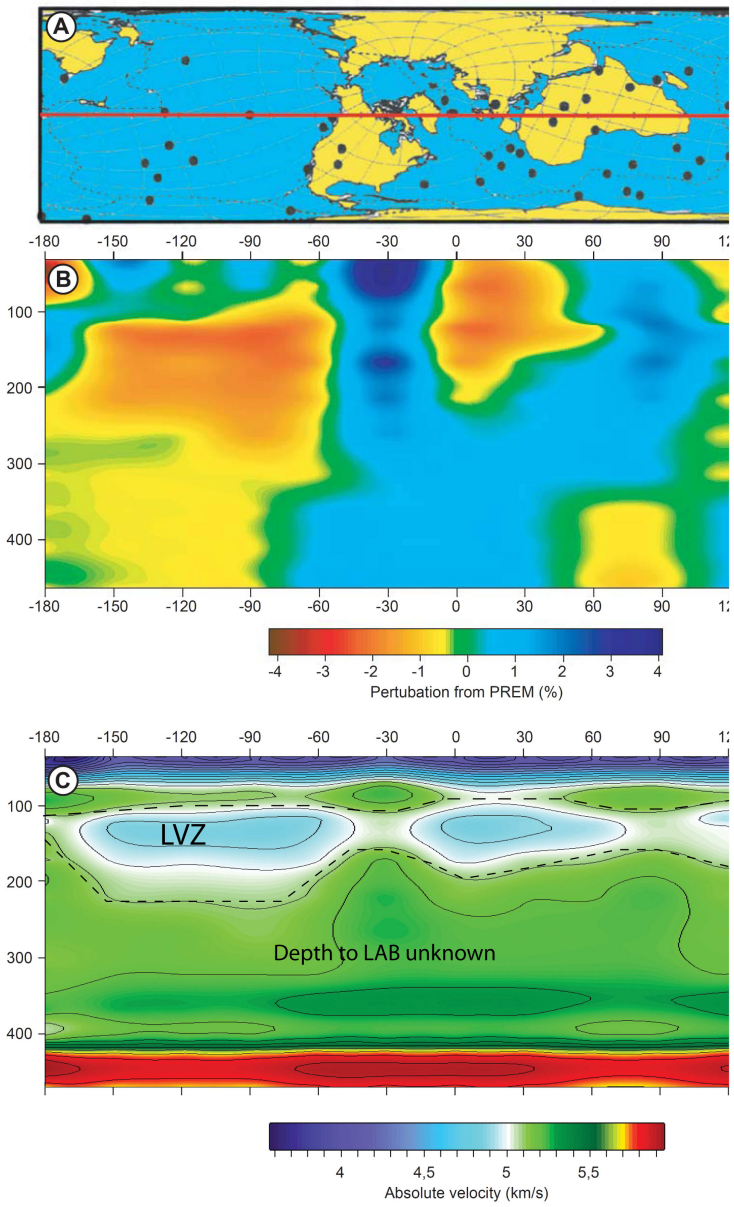

Figure 13: A global travel-time inversion (Zhang and Tanimoto, 1993). A) Map of the cross-section profile, B) wave-speed perturbations relative to the background model (PREM). This figure does not show any indication of an upper-mantle low-wave-speed zone. Instead it shows abrupt wave-speed discontinuities between continents and oceans. C) Absolute wave speeds calculated by adding the perturbations to the background model. This figure clearly shows a pronounced, global, low-wave-speed zone which is strongest beneath the oceans and extends into the continents. This feature is not seen in B). The amplitude of the anomaly in terms of absolute

wave-speed may be over-estimated due to smearing and smoothing in the inversion procedure (modified from Thybo, 2006).

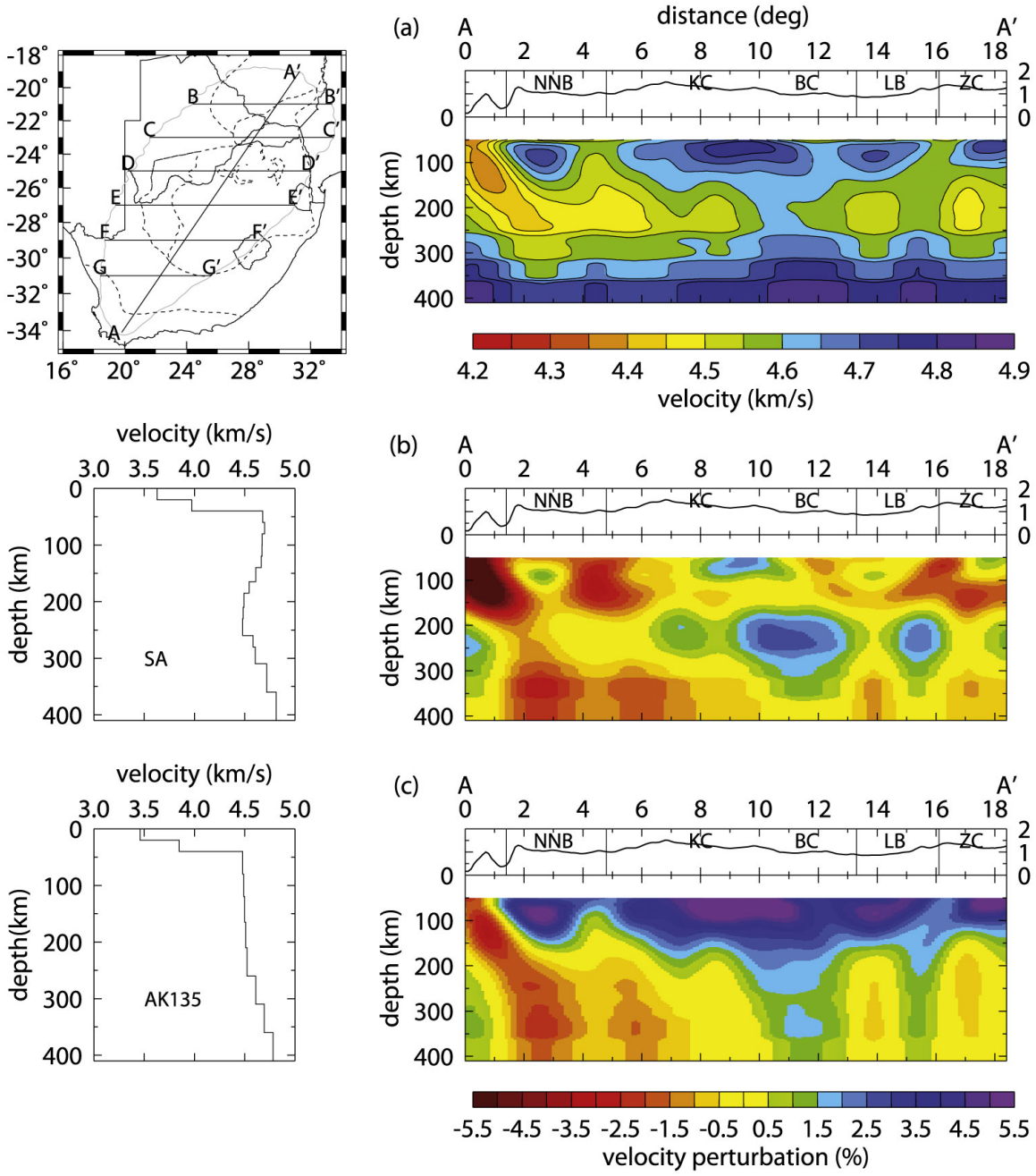

Figure 14: Absolute wave speed and wave-speed perturbation profiles across southern Africa. (a) Wave-speed profile along A-A' (map at left). (b) Wave-speed perturbation profile of A-A' relative to the average shear wave speed in southern Africa (left). (c) Wave-speed perturbation profile of A-A' relative to the standard global model AK135 (Kennett, et al., 1995, left). Topography is plotted above the wave-speed- and wave-speed perturbation profiles. Vertical lines indicate tectonic boundaries (from Li and Burke, 2006).

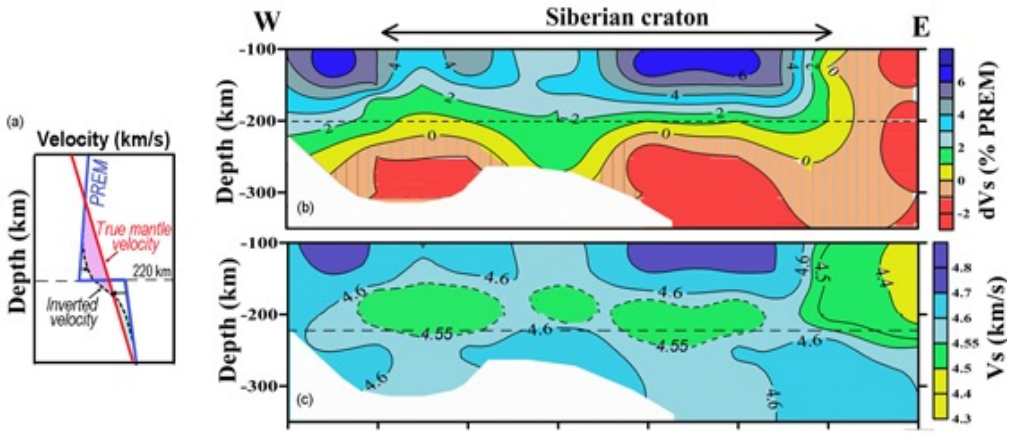

Figure 15: Using PREM (Dziewonski and Anderson, 1981) as a reference model in tomographic inversions for continental regions may lead to erroneous interpretations of the thickness of the seismic lithosphere (after Artemieva, 2011). (a) Sketch illustrating how the inversion result (dashed line) tends to 'smooth' the step at 220 km depth (a step not required for the continental mantle) by increasing wave speeds above (and decreasing wave speeds below) 220 km depth, thus artificially enhancing the velocity gradient across 220 km depth. Nonetheless, wave speeds remain lower than true mantle wave speeds above 220 km and higher below. (b, c) Wave-speed structure of the upper mantle beneath Siberia. Top: Relative v_S perturbations with respect to PREM based on Rayleigh-wave tomography and interpreted as evidence of a 200-km-thick lithosphere beneath the Siberian craton (Priestley and Debayle, 2003). Bottom: the same wave-

speed model recalculated to absolute velocities provides no evidence for the base of the lithosphere above 300 km, and it inherits from PREM the reduced wave-speed layer above 220 km (Artemieva, 2011).

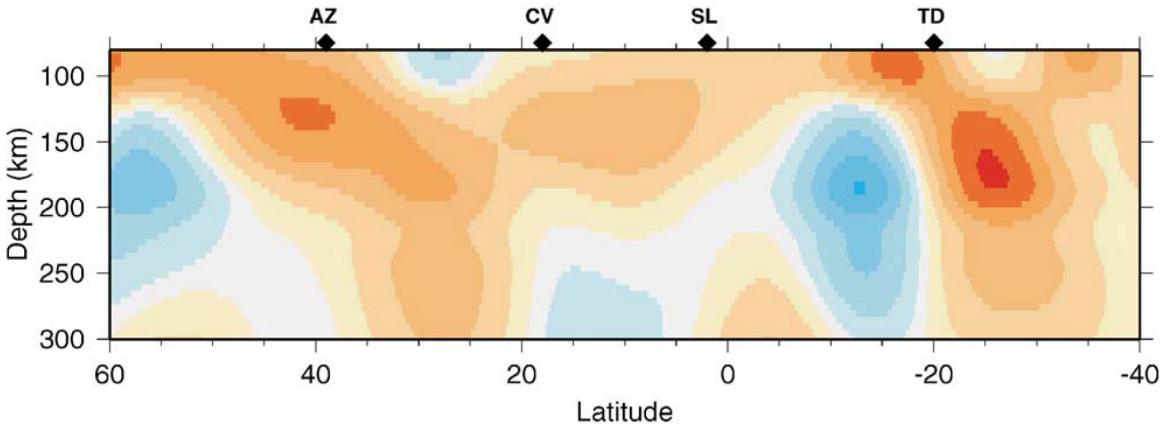

Figure 16: Cross-section of mantle v_S structure from surface-wave tomography, along longitude 24˚W, passing close to the Azores, Cape Verde, Sierra Leone and Tristan da Cunha. The vertical exaggeration of 14 makes quasi-horizontal regions of low seismic wave speed appear to be quasi-vertical (from Silveira and Stutzmann, 2002).

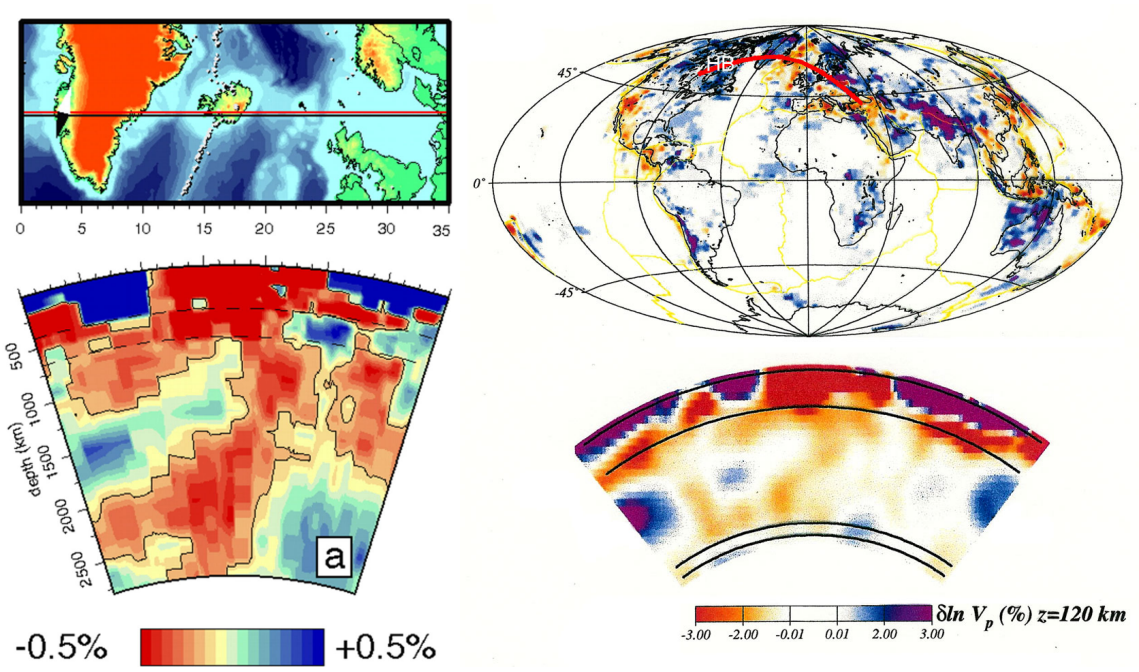

Figure 17: Left: whole-mantle tomography model. The cross section shown in (a) purports to show a mantle plume extending from the surface down to the core-mantle boundary under the North Atlantic (from Bijwaard and Spakman, 1999). Right: The same model, re-plotted with the color scale saturated at an anomaly strength of ±3%, and the line of section extended to underlie Canada and Scandinavia. HB: Hudson Bay. In the figure at left, saturation of the color scale at ±0.5% gives the impression that a low-wave-speed structure of roughly constant strength traverses the entire mantle, and truncation of the section at Greenland conceals the very similar structure imaged beneath Hudson Bay.

References

Achauer, U., Maguire, P.K.H., Mechie, J., Green, W.V. and group, t.K.w., 1992. Some Remarks On The Structure And Geodynamics Of The Kenya Rift, Tectonophysics, 213, 257-268.

Ádám, A. and Panza, G.F., 1989. A critical review of the magnetotelluric information on the upper mantle, Acta Geod. Geoph. Mont. Hung., 24, 395-415.

Agostini, S., Doglioni, C., Innocenti, F., Manetti, P. and Tonarini, S., 2010. On the geodynamics of the Aegean rift, Tectonophysics, 488, 7-21.

Aki, K., Christoffersson, A. and Husebye, E., 1977. Determination of the three-dimensional seismic structure of the lithosphere, Journal of Geophysical Research, 82, 277-296.

Aki, K. and Richards, P.G., 2002. Quantitative Seismology. University Science Books, Sausalito, California.

Alinaghi, A., Koulakov, I. and Thybo, H., 2007. Seismic tomographic imaging of P- and S-waves velocity perturbations in the upper mantle beneath Iran, Geophysical Journal International, 169, 1089-1102.

Amaru, M., Spakman, W., Villasenor, A., Sandoval, S. and Kissling, E., 2008. A new absolute arrival time data set for Europe, Geophysical Journal International, 173, 465-472.

Anderson, D.L., 1965. Recent evidence concerning the structure and composition of the Earth's mantle. In: Physics and Chemistry of the Earth 6 (L.H. Ahrens, J.B. Dawson, S.K. Runcorn and H.C. Urey, eds). Pergamon Press, Oxford.

Anderson, D.L., 1967. Phase changes in the upper mantle, Science, 157, 1165-1173.

Anderson, D.L., 2007. New Theory of the Earth. Cambridge University Press, Cambridge.

Anderson, D.L., 2011. Hawaii, boundary layers and ambient mantle–geophysical constraints, Journal of Petrology.

Arrowsmith, S., Kendall, J.-M., White, N. and VanDecar, J., 2005. Seismic imaging of a hot upwelling beneath the British Isles, Geology, 33, 345-348.

Artemieva, I.M., 2007. Dynamic topography of the East European Craton: shedding light upon the lithospheric structure, composition and mantle dynamics, Global and Planetary Change, 58, 411-434.

Artemieva, I.M., 2009. The continental lithosphere: reconciling thermal, seismic, and petrologic data, Lithos, 109, 23-46.

Artemieva, I.M., 2011. The lithosphere: An interdisciplinary approach. Cambridge Univ. Press.

Backus, G. and Gilbert, F., 1970. Uniqueness in the inversion of gross Earth data, Phil. Trans. Royal Soc. London, A266, 123-192.

Backus, G.E. and Gilbert, F., 1967. Numerical applications of a formalism for geophysical inverse problems, Geophysical Journal of the Royal Astronomical Society, 13, 247-276.

Backus, G.E. and Gilbert, F., 1968. The resolving power of gross earth data, Geophysical Journal of the Royal Astronomical Society, 16, 169-205.

Bailey, D.K., 1992. Episodic alkaline igneous activity across Africa, Magmatism and the Causes of Continental Breakup, 68, 91-98.

Bailey, D.K. and Woolley, A.R., 2005. Repeated, synchronous magmatism within Africa: timing, magnetic reversals and global tectonics. In: Plates, Plumes & Paradigms (G.R. Foulger, J.H. Natland, D.C. Presnall and D.L. Anderson, ed. Geological Society of America.

Bassin, C., Laske, G. and Masters, G., 2000. The current limits of resolution for surface wave tomography in North America, EOS Trans AGU, 81.

Bastow, I.D., 2012. Relative arrival-time upper-mantle tomography and the elusive background mean, Geophysical Journal International, 190, 1271–1278.

Bastow, I.D., Nyblade, A.A., Stuart, G.W., Rooney, T. and Benoit, M.H., 2008. Upper Mantle Seismic Structure Beneath the Ethiopian Hotspot: Rifting at the Edge of the African Low Velocity Anomaly, Geochemistry Geophysics Geosystems, 9.

Bastow, I.D., Stuart, G.W., Kendall, J.-M. and Ebinger, C.J., 2005. Upper-mantle seismic structure in a region of incipient continental breakup: northern Ethiopian rift, Geophysical Journal International, 162, 479-493.

Becker, T.W., 2012. On recent seismic tomography for the western United States, Geochemistry Geophysics Geosystems, 13.

Bijwaard, H. and Spakman, W., 1999. Tomographic evidence for a narrow whole mantle plume below Iceland, EPSL, 166, 121-126.

Billien, M., Lévêque, J.-J. and Trampert, J., 2000. Global maps of Rayleigh wave attenuation for periods between 40 and 150 seconds, Geophysical Research Letters, 27, 3619–3622.

Bonatti, E., 1990. Not so hot "hot spots" in the oceanic mantle, Science, 250, 107-111.

Boschi, L. and Ekstrom, G., 2002. New images of the upper mantle from measurements of surface wave phase velocity anomalies, Journal of Geophysical Research, 107.

Boven, A., Pasteels, P., Punzalan, L.E., Yamba, T.K. and Musisi, J.H., 1998. Quaternary perpotassic magmatism in Uganda (Toro-Ankole volcanic Province): age assessment and significance for magmatic evolution along the East African Rift, Journal of African Earth Science, 26, 463-476.

Boyadzhiev, G., Brandmayr, E., Pinat, T. and Panza, G.F., 2008. Optimization for non-linear inverse problems, Rendiconti Lincei, 19, 17-43.

Brandmayr, E., Marson, I., Romanelli, F. and Panza, G.F., 2011. Lithosphere density model in Italy: no hint for slab pull, Terra Nova, 23, 292-299.

Brandmayr, E., Raykova, R., Zuri, M., Romanelli, F., Doglioni, C. and Panza, G.F., 2010. The lithosphere in Italy: structure and seismicity. In: The Geology of Ital (M. Beltrando, A. Peccerillo, M. Mattei, S. Conticelli and C. Doglioni, eds).

Bruneton, M., Pedersen, H.A., Vacher, P., Kukkonen, I.T., Arndt, N.T., Funke, S., Friederich, W.g. and Farra, V., 2004. Layered lithospheric mantle in the central Baltic Shield from surface waves and xenolith analysis, Earth and Planetary Science Letters, 226, 41-52.

Cadoux, A., Blichert-Toft, J., Pinti, D.L. and Albarède, F., 2007. A unique lower mantle source for Southern Italy volcanics, Earth and Planetary Science Letters, 259, 227-238.

Cammarano, F., Goes, S., Vacher, P. and Giardini, D., 2003. Inferring upper mantle temperatures from seismic velocities, Physics of the Earth and Planetary Interiors, 138, 197-222.

Cammarano, F. and Romanowicz, B., 2007. Insights into the nature of the transition zone from physically constrained inversion of long period seismic data, PNAS-High Pressure Geoscience, 104, 9139-9144.

Cammarano, F., Tackley, P. and Boschi, L., 2011. Seismic, petrological and geodynamical constraints on thermal and compositional structure of the upper mantle: global thermo-chemical models, Geophysical Journal International, 187, 1301-1318.

Cao, Q., Van der Hilst, R.D., De Hoop, M.V. and Shim, S.-H., 2011. Seismic imaging of transition zone discontinuities suggests hot mantle west of Hawaii, Science, 332, 1068-1071.

Cara, M., 1979. Lateral variations of S-velocity in the upper mantle from higher Rayleigh modes, Geophysical Journal of the Royal Astronomical Society, 5, 649-670.

Carminati, E. and Doglioni, C., 2010. North Atlantic geoid high, volcanism and glaciations, Geophysical Research Letters, 37.

Carminati, E., Lustrino, M. and Doglioni, C., 2012. Geodynamic evolution of the central and western Mediterranean: Tectonics vs. igneous petrology constraints, Tectonophysics, in press.

Chen, G., Spetzler, H.A., Gettinag, I.C. and Yoneda, A., 1996. Selected elastic moduli and their temperature derivatives for olivine and garnet with different Mg/(Mg+Fe) contents: Results from GHz ultrasonic interferometry, Geophysical Research Letters, 23, 5-8.

Chen, Y.D., 1996. Constraints on melt production rate beneath the mid-ocean ridges based on passive flow models, Pure and Applied Geophysics, 146, 589-620.

Christoffersson, A. and Husebye, E.S., 2011. Seismic tomographic mapping of the Earth's interior — Back to basics revisiting the ACH inversion, Earth-Science Reviews, 106, 293–306.

Constable, S.C., Parker, R.L. and Constable, C.G., 1987. Occam's inversion: a practical algorithm for generating smooth models from electromagnetic sounding data, Geophysics, 52, 289–300.

Corchete, V. and Chourak, M., 2010. Shear-wave velocity structure of the western part of the Mediterranean Sea from Rayleigh-wave analysis, International Journal of Earth Science (Geol. Rundsch.), 99, 955–972.

Corchete, V. and Chourak, M., 2011. Shear-wave velocity structure of the south-eastern part of the Iberian Peninsula from Rayleigh wave analysis, International Journal of Earth Science (Geol. Rundsh.), 100, 1733–1747.

Courtillot, V., Davaillie, A., Besse, J. and Stock, J., 2003. Three distinct types of hotspots in the Earth's mantle, Earth and Planetary Science Letters, 205, 295-308.

Curtis, A., Trampert, J. and Snieder, R., 1998. Eurasian fundamental mode surface wave phase velocities and their relationship with tectonic structures, Journal of Geophysical Research, 103, 26919-26947.

Dahlen, F.A., Hung, S.-H. and Nolet, G., 2000. Frechet kernels for finite-frequency traveltimes – I. Theory, Geophysical Journal International, 141, 157-174.

Dahlen, F.A. and Tromp, J., 1998. Theoretical Global Seismology. Princeton University Press, Princeton, New Jersey.

Darbyshire, F.A., 2005. Upper mantle structure of Arctic Canada from Rayleigh wave dispersion, Tectonophysics, 405, 1-23.

Davies, J.H. and Bunge, H.-P., 2006. Are splash plumes the origin of minor hotspots?, Geology, 34, 349-352.

Debayle, E., Kennett, B.L.N. and Priestley, K.F., 2005. Global azimuthal seismic anisotropy and the unique plate-motion deformation of Australia, Nature, 433, 509–512.

Deschamps, F. and Trampert, J., 2004. Towards a lower mantle reference temperature and composition, Earth and Planetary Science Letters, 222, 161-175.

Deuss, A., 2009. Global Observations of Mantle Discontinuities Using SS and PP Precursors, Surv. Geophys., 30, 301–326.

Doglioni, C., Green, D.H. and Mongelli, F., 2005. On the shallow origin of hotspots and the westward drift of the lithosphere. In: Plates, Plumes, and Paradigms (G.R. Foulger, J.H. Natland, D.C. Presnall and D.L. Anderson, ed. Geological Society of America, Boulder, Colorado.

Du, Z. and Panza, G.F., 1999. Amplitude and phase differentiation of synthetic seismograms: a must for waveform inversion at regional scale, Geophysical Journal International, 136, 83–98.

Duggen, S., Hoernle, K.A., Hauff, F., Klugel, A., Bouabdellah, M. and Thirlwall, M.F., 2009. Flow of Canary mantle plume material through a subcontinental lithospheric corridor beneath Africa to the Mediterranean, Geology, 37, 283-286.

Dziewonski, A.M., 1971. On regional differences in dispersion of mantle Rayleigh waves, Geophysical Journal of the Royal Astronomical Society, 22, 289-326.

Dziewonski, A.M., 1971. Upper mantle models from “pure-path” dispersion data, Journal of Geophysical Research, 76, 2587–2601.

Dziewonski, A.M. and Anderson, D.L., 1981. Preliminary Reference Earth Model, Physics of the Earth and Planetary Interiors, 25, 297-356.

Ebinger, C.J. and Sleep, N.H., 1998. Cenozoic magmatism throughout East Africa resulting from impact of a single plume, nature, 395, 1788-1791.

Eby, G.N., Lloyd, F.E. and Woolley, A.R., 2009. Geochemistry and petrogenesis of the Fort Portal, Uganda, extrusive carbonatite, Lithos, 113, 785-800.

Eken, T., Shomali, Z.H., Roberts, R., Hieronymus, C.F. and Bodvarsson, R., 2008. S and P velocity heterogeneities within the upper mantle below the Baltic Shield, Tectonophysics, 462, 109-124.

Ekström, G., Tromp, J. and Larson, E.W.F., 1997. Measurements and global models of surface wave propagation, Journal of Geophysical Research, 102, 8137–8157.

Ellsworth, W.L., 1977. Three-dimensional structure of the crust and mantle beneath the island of Hawaii. Ph.D., Massachusetts Institute of Technology, 327 p.

Evans, J.R. and Achauer, U., 1993. Teleseismic velocity tomography using the ACH method: theory and application to continental-scale studies. In: Seismic Tomography: Theory and Applications (H.M. Iyer and K. Hirahara, eds). Chapman and Hall, London.

Evans, J.R. and Zucca, J.J., 1993. Active source, high-resolution (NeHT) tomography: velocity and Q. In: Seismic Tomography: Theory and Applications (H.M. Iyer and K. Hirahara, eds). Chapman and Hall, London.

Faccenna, C. and Beker, T.W., 2010. Shaping mobile belts by small-scale convection, Nature, 465, 602-605.

Farnetani, C., Hofmann, A.W. and Class, C., 2012. How double volcanic chains sample geochemical anomalies from the lowermost mantle, Earth and Planetary Science Letters, 359-360, 240-247.

Faul, U.H. and Jackson, I., 2007. Diffusion creep of dry, melt-free olivine, Journal of Geophysical Research, 112.

Feng, M., Lee, S.v.d. and Assumpcao, M., 2007. Upper mantle structure of South America from joint inversion of waveforms and fundamental mode group velocities of Rayleigh waves, Journal of Geophysical Research, 112.

Forte, A.M. and Perry, A.C., 2000. Seismic-geodynamic evidence for a chemically depleted continental tectosphere, Science, 290, 1940-1944.

Foulger, G.R., Miller, A.D., Julian, B.R. and Evans, J.R., 1995. Three-dimensional Vp and Vp/Vs structure of the Hengill triple junction and geothermal area, Iceland, and the repeatability of tomographic inversion, Geophysical Research Letters, 22, 1309-1312.

Foulger, G.R., Pritchard, M.J., Julian, B.R., Evans, J.R., Allen, R.M., Nolet, G., Morgan, W.J., Bergsson, B.H., Erlendsson, P., Jakobsdottir, S., Ragnarsson, S., Stefansson, R. and Vogfjord, K., 2001. Seismic tomography shows that upwelling beneath Iceland is confined to the upper mantle, Geophysical Journal International, 146, 504-530.

Frederiksen, A.W., Miong, S.-K., Darbyshire, F.A., Eaton, D.W., Rondenay, S. and Sol, S., 2007. Lithospheric variations across the Superior Province, Ontario, Canada: Evidence from tomography and shear wave splitting, Journal of Geophysical Research, 112.

Furman, T., 2007. Geochemistry of East African Rift basalts: an overview, Journal of African Earth Science, 48, 147-160.

Gibson, S.A., Thompson, R.N., Leonardos, O.H., Dickin, A.P. and Mitchell, J.G., 1995. The Late Cretaceous impact of the Trinidade mantle plume: Evidence from large volume, mafic potassic magmatism in SE Brazil, J Petrol, 36, 189-229.

Goes, S., Govers, R. and Vacher, P., 2000. Shallow mantle temperatures under Europe from *P* and *S* wave tomography, JGR, 105, 11,153-111,169.

Gomer, B.M. and Okal, E.A., 2003. Multiple-ScS probing of the Ontong-Java Plateau, Earth and Planetary Science Letters, 138, 317-331.

Gonzales, O., Alvarez, L., Moreno, B. and Panza, G.F., 2011. S-Wave Velocities of the Lithosphere-Asthenosphere System in the Caribbean Region, Pure and Applied Geophysics.

Grand, S.P., Van Der Hilst, R.D. and Widiyantoro, S., 1997. Global seismic tomography: A snapshot of convection in the Earth, GSA Today, 7, 1-7.

Green, D.H., Hibberson, W.O., Kovacs, I. and Rosenthal, A., 2010. Water and its influence on the lithosphere-asthenosphere boundary, Nature, 467, 448-452.

Green, W.V., Achauer, U. and Meyer, R.P., 1991. A 3-Dimensional Seismic Image of the Crust and Upper Mantle Beneath the Kenya Rift, Nature, 354, 199-203.

Gregersen, S., Voss, P. and Group, T.W., 2002. Summary of project TOR: delineation of a stepwise, sharp, deep lithosphere transition across Germany-Denmark-Sweden, Tectonophysics, 360, 61-73.

Gu, Y.J., Dziewonski, A.M. and Ekstrom, G., 2001. Preferential detection of the Lehmann discontinuity beneath continents, Geophysical Research Letters, 24, 4655– 4658.

Gu, Y.J., Dziewonski, A.M., Weijia, S. and Ekstrom, G., 2001. Models of the mantle shear velocity and discontinuities in the pattern of lateral heterogeneities, Journal of Geophysical Research, 106, 11,169–111,199.

Guarino, V., Vu, F.-W., Lustrino, M., Melluso, L., Brotzu, P., Gomes, C.B., Ruberti, E., Tassinari, C.C.G. and Svisero, D.P., in press. U–Pb ages, Sr–Nd- isotope geochemistry,

and petrogenesis of kimberlites, kamafugites and phlogopite-picrites of the Alto Paranaíba Igneous Province, Brazil, Chemical Geology.

Gung, Y., Panning, M.P. and Romanowicz, B., 2003. Global anisotropy and the thickness of continents, Nature, 422, 707-711.

Hamilton, W.B., 2007. Driving mechanism and 3-D circulation of plate tectonics. In: Whence the Mountains? Inquiries into the Evolution of Orogenic Systems: A Volume in Honor of Raymond A. Price (J.W. Sears, T.A. Harms and C.A. Evenchick, eds). Geological Society of America, Boulder, CO.

Hamilton, W.B., 2011. Plate tectonics began in Neoproterozoic time, and plumes from deep mantle have never operated, Lithos, 123, 1-20.

Handy, M.R., Schmid, S.M., Bousquet, R., Kissling, E. and Bernoulli, D., 2010. Reconciling platetectonic reconstructions of Alpine Tethys with the geological–geophysical record of spreading and subduction in the Alps, Earth-Science Reviews, 102, 121-158.

Hier-Majumder, S. and Courtier, A., 2011. Seismic signature of small melt fraction atop the transition zone, Earth and Planetary Science Letters, 308, 334-342.

Hofmann, A.W., 1988. Chemical differentiation of the Earth: the relationship between mantle, continental crust, and oceanic crust, Earth and Planetary Science Letters, 90, 297-314.

Hofmann, A.W., 1997. Mantle geochemistry: the message from oceanic volcanism, Nature, 385, 219-229.

Hofmann, A.W., 2003. Sampling mantle heterogeneity through oceanic basalts: Isotopes and trace elements. In: Treatise on Geochemistry: The Mantle and Core (R.W. Carlson, H.D. Holland and K.K. Turekian, eds). Elsevier.

Hung, S.-H., Dahlen, F.A. and Nolet, G., 2001. Wavefront healing: a banana-doughnut perspective, Geophysical Journal International, 146.

Hung, S.-H., Shen, Y. and Chiao, L.-Y., 2004. Imaging seismic velocity structure beneath the Iceland hotspot - A finite-frequency approach, Journal of Geophysical Research, 109.

Ishii, M. and Tromp, J., 2004. Constraining large-scale mantle heterogeneity using mantle and inner-core sensitive normal modes, Physics of the Earth and Planetary Interiors, 146, 113-124.

Jackson, M.G., Carlson, R.W., Kurz, M.D., Kempton, P.D., Francis, D. and Blusztajn, J., 2010. Evidence for the survival of the oldest terrestrial mantle reservoir, Nature, 466, 853-856.

James, D.E., Niu, F.L. and Rokosky, J., 2003. Crustal structure of the Kaapvaal craton and its significance for early crustal evolution, Lithos, 71, 413-429.

Jordan, T.H., 1975. The continental tectosphere, Reviews of Geophysics and Space Physics, 13, 1-13.

Jordan, T.H., 1979. Mineralogies, densities and seismic velocities of garnet lherzolites and their geophysical implications. In: The Mantle Sample: Inclusions in Kimberlites and Other Volcanics (F.R. Boyd and H.O.A. Meyer, eds). American Geophysical Union, Washington.

Julian, B.R., 2005. What can seismology say about hot spots? In: Plates, Plumes, and Paradigms (G.R. Foulger, J.H. Natland, D.C. Presnall and D.L. Anderson, ed. Geological Society of America.

Julian, B.R. and Evans, J.R., 2010. On possible plume-guided seismic waves, Bulletin of the Seismological Society of America, 100, 497-508.

Julian, B.R. and Foulger, G.R., 2013. Using distant sources in local earthquake tomography, Geophysical Journal International, submitted to Geophysical Journal International.

Kaban, M.K., Schwintzer, P., Artemieva, I.M. and Mooney, W.D., 2003. Density of the continental roots: compositional and thermal effects, Earth and Planetary Science Letters, 209, 53-69.

Karato, S.-I. and Karki, B.B., 2001. Origin of lateral variation of seismic wave and velocities and density in the deep mantle, Journal of Geophysical Research, 106, 21771–21783.

Katzman, R., Zhao, L. and Jordan, T.H., 1998. High-resolution, twodimensional vertical tomography of the central Pacific mantle using ScS reverberations and frequency-dependent travel times, Journal of Geophysical Research, 103, 17933-17971.

Keller, W.R., Anderson, D.L. and Clayton, R.W., 2000. Resolution of tomographic models of the mantle beneath Iceland, Geophysical Research Letters, 27, 3993-3996.

Kellogg, L.H., Hager, B.H. and Van Der Hilst, R.D., 1999. Compositional stratification in the deep mantle, Science, 283, 1881-1884.

Kellogg, L.H. and Wasserburg, G.J., 1990. The role of plumes in mantle helium fluxes, Earth and Planetary Science Letters, 99, 276-289.

Kelly, R.K., Kelemen, P.B. and Jull, M., 2003. Buoyancy of the continental upper mantle, Geochemistry Geophysics Geosystems, 4, 1017.

Kennett, B.L.N., 2006. On seismological reference models and the perceived nature of heterogeneity, Physics of the Earth and Planetary Interiors, 159, 129-139.

Kennett, B.L.N. and Engdahl, E.R., 1991. Travel times for global earthquake location and phase identification, GJI, 105, 429-466.

Kennett, B.L.N., Engdahl, E.R. and Buland, R., 1995. Constraints on seismic velocities in the Earth from traveltimes, Geophysical Journal International, 122, 108-124.

Kennett, B.L.N., Widiyantoro, S. and Hilst, R.D.v.d., 1998. Joint seismic tomography for bulk sound and shear wave speed in the Earth's mantle, Journal of Geophysical Research, 103, 12,469-412,494.

Kern, H., 1978. The effect of high temperature and high confining pressure on compositional wave velocities in quartz-bearing and quartz-free igneous and metamorphic rocks, Tectonophysics, 44, 185-203.

Klosko, E.R., Russo, R.M., Okal, E.A. and Richardson, W.P., 2001. Evidence for a rheologically strong chemical mantle root beneath the Ontong-Java Plateau, Earth and Planetary Science Letters, 186, 347-361.

Knopoff, L. and Panza, G.F., 1977. Resolution of upper mantle structure using higher modes of Rayleigh waves, Annales Geophysique, 30, 491-505.

Kuo, C. and Romanowicz, B., 2002. On the resolution of density anomalies in the Earth's mantle using spectral fitting of normal-mode data, Geophysical Journal International, 150, 162–179.

Kustowski, B., Ekström, G. and Dziewonski, A.M., 2008. The shear-wave velocity structure in the upper mantle beneath Eurasia, Geophysical Journal International, 174, 978–992.

Lebedev, S., Boonen, J. and Trampert, J., 2009. Seismic structure of Precambrian lithosphere: New constraints from broad-band surface-wave dispersion, Lithos, 109, 96-111.

Lebedev, S. and Hilst, R.D.v.d., 2008. Global upper-mantle tomography with the automated multimode inversion of surface and S-wave forms, Geophysical Journal International, 173, 505–518.

Lee, C.-T.A., 2003. Compositional variation of density and seismic velocities in natural peridotites at STP conditions: Implications for seismic imaging of compositional heterogeneities in the upper mantle, Journal of Geophysical Research, 108, 2441, doi:2410.1029/2003JB002413.

Legendre, C.P., Meier, T., Lebedev, S., Friederich, W. and Viereck-Gotte, L., 2012. A shear wave velocity model of the European upper mantle from automated inversion of seismic shear and surface waveforms, Geophysical Journal International, 191, 282-304.

Léveque, J.-J. and Masson, F., 1999. From ACH tomographic models to absolute velocity models, Geophysical Journal International, 137, 621-629.

Lévêque, J.J., Debayle, E. and Maupin, V., 1998. Anisotropy in the Indian Ocean upper mantle from Rayleigh- and Love-waveform inversion, Geophysical Journal International, 133, 529-540.

Léveque, J.J., Rivera, L. and Wittlinger, G., 1993. On the use of the checker-board test to assess the resolution of tomographic inversions, Geophysical Journal International, 115, 313-318.

Levshin, A.L.L., Schweitzer, J., Weidle, C., Shapiro, N. and Ritzwoller, M., 2007. Surface Wave Tomography of the Barents Sea and Surrounding Regions, Geophysical Journal International, 170, 441–459.

Li, A. and Burke, K., 2006. Upper mantle structure of southern Africa from Rayleigh wave tomography, Journal of Geophysical Research, 111.

Li, C., van der Hilst, R.D., Engdahl, E.R. and Burdick, S., 2008. A new global model for P wave speed variations in Earth's mantle, Geochemistry Geophysics Geosystems, 9.

Li, X.D. and Romanowicz, B., 1996. Global mantle shear velocity model developed using nonlinear asymptotic coupling theory, Journal of Geophysical Research, 101, 22,245-222,273.

Lippitsch, R., Kissling, E. and Ansorge, J., 2003. Upper mantle structure beneath the Alpine orogen from high-resolution teleseismic tomography, Journal of Geophysical Research, 108.

Lou, X., van der Lee, S. and Lloyd, S., 2013. AIMBAT: A Python/Matplotlib Tool for Measuring Teleseismic Arrival Times, Seismological Research Letters, 84, 85-93.

Lustrino, M., 2011. What ‘anorogenic’ igneous rocks can tell us about the chemical composition of the upper mantle: case studies from the circum-Mediterranean area, Geological Magazine, 148, 304-316.

Marone, F., Gung, Y.C. and Romanowicz, B., 2007. Three-dimensional radial anisotropic structure of the North American upper mantle from inversion of surface waveform data, Geophysical Journal International, 171, 206-222.

Masson, F. and Trampert, J., 1997. On ACH, or how reliable is regional teleseismic delay time tomography?, Physics of the Earth and Planetary Interiors, 102, 21-32.

Mavko, G.M., 1980. Velocity and attenuation in partially molten rocks, Journal of Geophysical Research, 85, 5173–5189.

McKenzie, D. and Priestley, K., 2008. The influence of lithospheric thickness variations on continental evolution, Lithos, 102, 1-11.

Medhus, A.B., Balling, N., Jacobsen, B.H., Weidle, C., England, R.W., Kind, R., Thybo, H. and Voss, P., 2012. Upper-mantle structure beneath the Southern Scandes Mountains and the Northern Tornquist Zone revealed by P-wave traveltime tomography, Geophysical Journal International, 189, 1315-1334.

Menke, W., 1984. Geophysical Data Analysis: Discrete Inverse Theory. Academic Press Inc.

Mierdel, K., Keppler, H., Smyth, J.R. and Langenhorst, F., 2007. Water solubility in aluminous orthopyroxene and the origin of Earth's asthenosphere, Science, 315, 354-368.

Montelli, R., Nolet, G., Dahlen, F. and Masters, G., 2006. A catalogue of deep mantle plumes: new results from finite-frequency tomography, Geochemistry Geophysics Geosystems, 7.

Montelli, R., Nolet, G., Dahlen, F.A., Masters, G., Engdahl, R.E. and Hung, S.-H., 2004. Finite frequency tomography reveals a variety of plumes in the mantle, Science, 303, 338-343.

Montelli, R., Nolet, G., Masters, G., Dahlen, F. and Hung, S.-H., 2004. Global P and PP traveltime tomography: rays versus waves, Geophysical Journal International, 158, 637–654.

Mooney, W.D., Laske, G. and Masters, T.G., 1998. CRUST 5.1: A global crustal model at 5° × 5°, Journal of Geophysical Research, 103, 727-747.

Mosegaard, K. and Tarantola, A., 2002. Probabilistic Approach to Inverse Problems. In: International Handbook of Earthquake & Engineering Seismology, Part A. Academic Press.

Murase, T. and Fukuyama, H., 1980. Shear wave velocity in partially molten peridotite at high pressures. In: Year Book Carnegie Institute, Washington, DC.

Murase, T. and Kushiro, I., 1979. Compressional wave velocity in partially molten peridotite at high pressures. In: Year Book Carnegie Institute, Washington, DC.

Murase, T., Kushiro, I. and Fujii, T., 1977. Compressional wave velocity in partially molten peridotite. In: Annual Report of the Director Geophysical Laboratory, Carnegie Inst., Washington D.C.

Muraveva, N.S. and Senin, V.G., 2009. Carbonate-silicate equilibria in the high-magnesia ultrapotassic volcanics of the Toro-Ankole Province (East African Rift Zone), Geochemistry International, 47, 882-900.

Nakanishi, I. and Anderson, D.L., 1984. Aspherical heterogeneity of the mantle from phase velocities of mantle waves, Nature, 307, 117-121.

Nataf, H.C., Nakanishi, I. and Anderson, D.L., 1984. Anisotropy and shear-velocity heterogeneities in the upper mantle, Geophysical Research Letters, 11, 109-112.

Ni, H., Keppler, H. and Behrens, H., 2011. Electrical conductivity of hydrous basaltic melts: implications for partial melting in the upper mantle, Contributions to Mineralogy and Petrology, 162, 637-650.

Nielsen, C. and Thybo, H., 2009. No Moho uplift below the Baikal Rift Zone: Evidence from a seismic refraction profile across southern Lake Baikal, Journal of Geophysical Research, 114.

Niu, Y., Collerson, K.D., Batiza, R., Wendt, J.I. and Regelous, M., 1999. Origin of enriched-type mid-ocean ridge basalt at ridges far from mantle plumes: The East Pacific Rise at 11˚20'N, Journal of Geophysical Research B: Solid Earth, 104, 7067-7087.

Nolet, G., 1985. Nolet, G., Solving or resolving inadequate and noisy tomographic systems, Journal of Computational Physics, 61, 463-482.

Nolet, G., 2008. A Breviary of Seismic Tomography. Cambridge University Press, Cambridge.

O'Donnell, J.P., Daly, E., Tiberi, C., Bastow, I.D., O'Reilly, B.M., Readman, P.W. and Hauser, F., 2011. Lithosphere-asthenosphere interaction beneath Ireland from joint inversion of teleseismic P-wave delay times and GRACE gravity, Geophysical Journal International, 184, 1379–1396.

Obrebski, M., Allen, R.M., Pollitz, F. and Hung, S.H., 2011. Lithosphere-asthenosphere interaction beneath the western United States from the joint inversion of body-wave

traveltimes and surface-wave phase velocities, Geophysical Journal International, 185, 1003-1021.

Oyarzun, R., 1997. Opening of the central Atlantic and asymmetric mantle upwelling phenomena: Implications for long-lived magmatism in western North Africa and Europe, Geology, 25, 727-730.

Paige, C.C. and Saunders, M.A., 1982. LSQR: an algorithm for sparse linear equations and sparse least squares, Assoc. Comput. Mach., Trans. Math. Software, 8, 43-71.

Panning, M.P., Lekic, V. and Romanowicz, B.A., 2010. The importance of crustal corrections in the development of a new global model of radial anisotropy, Journal of Geophysical Research, 115.

Panza, G.F., Doglioni, C. and Levshin, A., 2010. Asymmetric ocean basins, Geology, 38, 59-62.

Panza, G.F., Peccerillo, A., Aoudia, A. and Farina, B., 2007. Geophysical and petrological modelling of the structure and composition of the crust and upper mantle in complex geodynamic settings: the Tyrrhenian Sea and surroundings, Earth-Science Reviews, 80, 1-46.

Paul, A., Hatzfeld, D., Kaviani, A., Tatar, M. and Pequegnat, C., 2010. Seismic imaging of the lithospheric structure of the Zagros mountain belt (Iran). In: Tectonic and Stratigraphic Evolution of Zagros and Makran during the Mesozoic-Cenozoi (P. Leturmy and C. Robin, eds).

Pik, R., Marty, B. and Hilton, D.R., 2006. How many mantle plumes in Africa? The geochemical point of view, Chemical Geology, 226, 100-114.

Pilidou, S., Priestley, K., Gudmundsson, O. and Debayle, E., 2004. Upper mantle S-wave speed heterogeneity and anisotropy beneath the North Atlantic from regional surface wave tomography: the Iceland and Azores plumes, Geophysical Journal International, 159, 1057-1076.

Pilidou, S., Priestley, K.F., Debayle, E. and Gudmundsson, O., 2005. Rayleigh wave tomography in the North Atlantic: high resolution images of the Iceland, Azores and Eifel mantle plumes, Lithos, 79, 453-474.

Piromallo, C., Gasperini, D., Macera, P. and Faccenna, C., 2008. A late Cretaceous contamination episode of the European-Mediterraenan mantle, Earth and Planetary Science Letters, 268, 15-27.

Polet, J. and Anderson, D., 1995. Depth extent of cratons as inferred from tomographic studies, Geology, 23, 205-208.

Poupinet, G., 1979. On the relation between P-wave travel time residuals and the age of the continental plates, Earth and Planetary Science Letters, 43, 149-161.

Poupinet, G., Arndt, N. and Vacher, P., 2003. Seismic tomography beneath stable regions and the origin and composition of the continental lithospheric mantle, Earth and Planetary Science Letters, 212, 89-101.

Presnall, D. and Gudmundsson, G., 2011. Oceanic volcanism from the low-velocity zone – without mantle plumes, Journal of Petrology, 52, 1533-1546.

Priestley, K.F. and Debayle, E., 2003. Seismic evidence for a moderately thick lithosphere beneath the Siberian Platform, Geophysical Research Letters, 30, 1118-1122.

Priestley, K.F. and Tilmann, F., 2009. Relationship between the upper mantle high velocity seismic lid and the continental lithosphere, Lithos, 109, 112–124.

Rawlinson, N. and Fishwick, S., 2012. Seismic structure of the southeast Australian lithosphere from surface and body wave tomography, Tectonophysics, 572, 111-122.

Raykova, R.B. and Panza, G.F., 2010. The shear-wave velocity structure of the lithosphere-asthenosphere system in the Iberian area and surroundings. In: Rend. Fis. Acc. Lincei. Springer.

Ritsema, J., Heijst, H.J.v., Deuss, A. and Woodhouse, J.H., 2011. S40RTS: a degree-40 shear velocity model for the mantle from new Rayleigh wave dispersion, teleseismic traveltimes, and normal-mode splitting function measurements, Geophysical Journal International, 184, 1223–1236.

Ritsema, J., Heijst, H.J.v. and Woodhouse, J.H., 2004. Global transition zone tomography, Journal of Geophysical Research, 109.

Ritsema, J., van Heijst, H.J. and Woodhouse, J.H., 1999. Complex shear wave velocity structure imaged beneath Africa and Iceland, Science, 286, 1925-1928.

Ritter, J.R.R., Jordan, M., Christensen, U.R. and Achauer, U., 2001. A mantle plume below the Eifel volcanic fields, Germany, Earth and Planetary Science Letters, 186, 7-14.

Ritzwoller, M.H., Shapiro, N.M., Barmin, M.P. and Levshin, A.L., 2002. Global surface wave diffraction tomography, Journal of Geophysical Research, 107, 2335.

Ritzwoller, M.H., Shapiro, N.M., Levshin, A.L. and Leahy, G.M., 2001. Crustal and upper mantle structure beneath Antarctica and surrounding oceans, Journal of Geophysical Research, 106, 30645–30670.

Rosenthal, A., Foley, S.F., Pearson, D.G., Nowell, G.M. and Tappe, S., 2009. Petrogenesis of strongly alkaline primitive volcanic rocks at the propagating tip of the western branch of the East African Rift, Earth and Planetary Science Letters, 284, 236-248.

Rychert, C.A. and Shearer, P.M., 2009. A Global View of the Lithosphere-Asthenosphere Boundary, Science, 324, 495-498.

Saltzer, R.L., van der Hilst, R.D. and Karason, H., 2001. Comparing P and S wave heterogeneity in the mantle, Geophysical Research Letters, 28, 1335-1338.

Sambridge, M.S., 1999. Geophysical Inversion with a Neighbourhood Algorithm -I. Searching a parameter space, Geophysical Journal International, 138, 479-494.

Sambridge, M.S., 1999. Geophysical Inversion with a Neighbourhood Algorithm -II. Appraising the ensemble, Geophysical Journal International, 138, 727-746.

Scherstén, A., Elliott, T., Hawkesworth, C. and Norman, M., 2004. Tungsten isotope evidence that mantle plumes contain no contribution from the Earth's core, Nature, 427, 234-237.

Schmeling, H., 1985. Numerical model of partial melt on elastic, anelastic and electric properties of rocks, Part I. Elasticity and anelasticity, Physics of the Earth and Planetary Interiors, 41, 34-57.

Shapiro, N.M. and Ritzwoller, M.H., 2002. Monte-Carlo inversion for a global shear velocity model of the crust and upper mantle, Geophysical Journal International, 151, 88-105.

Shaw, H.R., 1973. Mantle convection and volcanic periodicity in the Pacific; evidence from Hawaii, Geological Society of America Bulletin, 84, 1505-1526.

Silveira, G. and Stutzmann, E., 2002. Anisotropic tomography of the Atlantic ocean, Physics of the Earth and Planetary Interiors, 132, 237-248.

Simons, F.J., Zielhuis, A. and van der Hilst, R.D., 1999. The deep structure of the Australian continent from surface wave tomography, Lithos, 48, 17-43.

Song, T.R.A. and Helmberger, D.V., 2007. Validating tomographic models with broad-band waveform modelling: an example from the LA RISTRA transect in the southwestern United States, Geophysical Journal International, 171, 244-258.

Spencer, C. and Gubbins, D., 1980. Travel-time inversion for simultaneous earthquake location and velocity structure determination in laterally varying media, Geophysical Journal of the Royal Astronomical Society, 63, 95-116.

Sramek, O., McDonough, W.F., Kite, E.K., Lekic, V., Dye, S.T. and Zhong, S., in press. Geophysical and geochemical constraints on geoneutrino fluxes from Earth's mantle, Earth and Planetary Science Letters.

Stracke, A., 2012. Earth's heterogeneous mantle: A product of convection-driven interaction between crust and mantle, Chemical Geology, 330-331, 274-299.

Stracke, A., Hofmann, A.W. and Hart, S.R., 2005. FOZO, HIMU, and the rest of the mantle zoo, Geochemistry Geophysics Geosystems, 6.

Stuart, F.M., Lass-Evans, S., Fitton, J.G. and Ellam, R.M., 2003. High 3He/4He ratios in picritic basalts from Baffin Island and the role of a mixed reservoir in mantle plumes, Nature, 424, 57-59.

Sumino, Y. and Anderson, O.L., 1982. Elastic constants in minerals. In: CRC Handbook of Physical Properties of Rocks (R.S. Carmichel, ed. CRC Press, Boca Raton, Fla.

Sun, D. and Helmberger, D., 2011. Upper-mantle structures beneath USArray derived from waveform complexity, Geophysical Journal International, 184, 416–438.

Tanimoto, T. and Anderson, D.L., 1984. Mapping convection in the mantle, Geophysical Research Letters, 11, 287-290.

Tappe, S., Foley, S.F. and Pearson, D.G., 2003. The kamafugites of Uganda: a mineralogical and geochemical comparison with their Italian and Brazilian analogues, Periodico di Mineralogia, 72, 51-77.

Tarantola, A., 1987. Inverse Problem Theory. Elsevier Science Ltd.

Thurber, C.H., 1993. Local earthquake tomography: velocities and Vp/Vs - theory. In: Seismic Tomography: Theory and Applications (H.M. Iyer and K. Hirahara, eds). Chapman and Hall, London.

Thybo, H., 2006. The heterogeneous upper mantle low velocity zone, Tectonophysics, 416, 53-79.

Thybo, H., Nielsen, L. and Perchuc, E., 2003. Seismic scattering at the top of the mantle transition zone, Earth and Planetary Science Letters, 216, 259-269.

Thybo, H. and Perchuc, E., 1997. The seismic 8˚ discontinuity and partial melting in continental mantle, Science, 275, 1626-1629.

Trampert, J., Deschamps, F., Resovsky, J. and Yuen, D., 2004. Probabilistic tomography maps chemical heterogeneities throughout the lower mantle, Science, 306, 853-856.

Trampert, J. and Spetzler, J., 2006. Surface wave tomography: finite frequency effects lost in the null space, Geophysical Journal International, 164, 394–400.

Trampert, J. and van der Hilst, R.D., 2005. Towards a quantitative interpretation of global seismic tomography, Geophysical Monograph, 160, 47-62.

Trampert, J. and Woodhouse, J.H., 1995. Global phase velocity maps of Love and Rayleigh waves between 40 and 150 s, Geophysical Journal International, 122, 675-690.

Tumanian, M., Frezzotti, M.L., Peccerillo, A., Brandmayr, E. and Panza, G.F., 2012. Thermal structure of the shallow upper mantle beneath Italy and neighbouring areas: Correlation with magmatic activity and geodynamic significance, Earth-Science Reviews, 114, 369-385.

van der Hilst, R., Engdahl, E.R. and Spakman, W., 1993. Tomographic inversion of P and pP data for aspherical mantle structure below the northwest Pacific region, Geophysical Journal International, 115, 264-302.

van der Hilst, R.D., 2004. Changing Views on Earth's Deep Mantle, Science, 306, 817-818.

van der Hilst, R.D. and de Hoop, M.V., 2005. Banana-doughnut kernels and mantle tomography, Geophysical Journal International, 163, 956-961.

van der Hilst, R.D. and Karason, H., 1999. Compositional heterogeneity in the bottom 1000 kilometers of Earth's mantle, Science, 283, 1881-1888.

van der Lee, S., James, D. and Silver, P., 2001. Upper mantle S velocity structure of central and western South America, Journal of Geophysical Research, 106, 30,821 – 830,834.

Van Der Lee, S. and Nolet, G., 1997. Seismic image of the subducted trailing fragments of the Farallon plate, Nature, 386, 266-269.

VanDecar, J.C., 1991. Upper-mantle structure of the Cascadia subduction zone from non-linear teleseismic traveltime inversion, University of Washington, Seattle.

VanDecar, J.C. and Crosson, R.S., 1990. Determination of teleseismic relative phase arrival times using multi-channel cross-correlation and least squares, BSSA, 80, 150-169.

VanDecar, J.C., James, D.E. and Assumpcao, M., 1995. Seismic evidence for a fossil mantle plume beneath south America and implications for plate driving forces, Nature, 378, 25-31.

Wawerzinek, B., Ritter, J.R.R., Jordan, M. and Landes, M., 2008. An upper-mantle upwelling underneath Ireland revealed from non-linear tomography, Geophysical Journal International, 175, 253-268.

Webber, A.P., Roberts, S., Taylor, R.N. and Pitcairn, I.K., 2013. Golden plumes: substantial gold enrichment of oceanic crust during ridge-plume interaction, Geology, 4187-90.

West, M., Gao, W. and Grand, S.P., 2004. A simple approach to the joint inversion of seismic body and surface waves applied to the southwest U.S., Geophysical Research Letters, 31.

White, W.M., 2010. Oceanic Island Basalts and mantle plumes: the geochemical perspective, Annual Review of Earth and Planetary Sciences, 38, 133-160.

Wolfe, C.J., Solomon, S.C., Laske, G., Collins, J.A., Detrick, R.S., Orcutt, J.A., Bercovici, D. and E.H. Hauri, 2011. Mantle P-wave velocity structure beneath the Hawaiian hotspot, Earth and Planetary Science Letters, 303, 267-280.

Wolfe, C.J., Solomon, S.C., Laske, G., Collins, J.A., Detrick, R.S., Orcutt, J.A., Bercovici, D. and Hauri, E.H., 2009. Mantle shear-wave velocity structure beneath the Hawaiian hot spot, Science, 326, 1388-1390.

Woodhouse, J.H. and Dziewonski, A.M., 1984. Mapping the upper mantle: Three-dimensional modeling of Earth structure by inversion of seismic waveforms, Journal of Geophysical Research, 89, 5953–5986.

Wyllie, P.J., 1988. Magma genesis, plate tectonics and chemical differentiation of the Earth, Rev. Geophys., 26, 370-404.

Yang, Y., Ritzwoller, M.H., Levshin, A.L. and Shapiro, N.M., 2007. Ambient noise Rayleigh wave tomography across Europe, Geophysical Journal International, 168, 259–274.

Yanovskaya, T.B., 1997. Resolution estimation in the problems of seismic ray tomography, Izvestiya, Physics of the Solid Earth, 33, 762-765.

Yanovskaya, T.B., 2009. Surface wave tomography method based on data from distant earthquakes, Izvestiya, Physics of the Solid Earth, 45, 225-230.

Yanovskaya, T.B. and Kozhevnikov, V.M., 2003. 3D S-wave velocity pattern in the upper mantle beneath the continent of Asia from Rayleigh wave data, Physics of the Earth and Planetary Interiors, 138, 263-278.

Yuan, H. and Dueker, K.G., 2005. Teleseismic P-wave tomogram of the Yellowstone plume, Geophysical Research Letters, 32.

Zhang, Y.S. and Tanimoto, T., 1993. High-resolution global upper mantle structure and plate tectonics, Journal of Geophysical Research, 98, 9793–9823.

Zhou, H. and Dick, H.J.B., 2013. Thin crust as evidence for depleted mantle supporting the Marion Rise, Nature.

Zhou, Y., Nolet, G., Dahlen, F.A. and Laske, G., 2006. Global upper-mantle structure from finite-frequency surface-wave tomography, Journal of Geophysical Research, 111.

Zindler, A. and Hart, S.R., 1986. Chemical Geodynamics, Ann Rev Earth Plan Sci, 14, 493-571.